UNCLASSIFIED

AD **433961**

DEFENSE DOCUMENTATION CENTER

FOR

SCIENTIFIC AND TECHNICAL INFORMATION

CAMERON STATION. ALEXANDRIA. VIRGINIA

UNCLASSIFIED

AL-TDR-64-37

64-11

GASEOUS OPTICAL MASERS

TECHNICAL DOCUMENTARY REPORT NO. AL-TDR-64-37

December 1963

Air Force Avionics Laboratory
Aeronautical Systems Division
Air Force Systems Command
Wright-Patterson Air Force Base, Ohio

Project 4156, Task No. 415608

NOTICES

When Government drawings, specifications, or other data are used for any purpose other than in connection with a definitely related Government procurement operation, the United States Government thereby incurs no responsibility nor any obligation whatsoever; and the fact that the Government may have formulated furnished, or in any way supplied the said drawings, specifications, or other data, is not to be regarded by implication or otherwise as in any manner licensing the holder or any other person or corporation, or conveying any rights or permission to manufacture, use, or sell any patented invention that may in any way be related thereto.

AL-TDR-64-37

GASEOUS OPTICAL MASERS

TECHNICAL DOCUMENTARY REPORT NO. AL-TDR-64-37

December 1963

Air Force Avionics Laboratory
Aeronautical Systems Division
Air Force Systems Command
Wright-Patterson Air Force Base, Ohio

Project 4156, Task No. 415608

NOTICES

FOREWORD

This report was prepared by Watkins-Johnson Company under USAF Contract No.
AF 33(657)-8986. The contract was initiated under Project No. 4156, Task No. 415608.
The work was administered under the direction of the Directorate of Avionics,
Aeronautical Systems Division, Messrs. M. Heil and R. Firsdon, project engineers.

This report covers work conducted from May 1962 to November 1963. The principal
investigator at Watkins-Johnson Company was Dr. S. E. Sobottka, with many contri-
butions from Dr. V. Met.

ABSTRACT

Studies were made of basic processes operating in He-Ne lasers with emphasis on acquiring information related to techniques for increasing the output powers. It was found that the population of the upper maser level for the 6328A and 1.15μ transitions saturates with increasing electron density or energy as is predicted for excitation by resonance transfer from He metastables. The population of the lower maser level for the 6328A transition does not saturate so that the laser output power, as a function of electron density, increases to a maximum and then decreases to zero. Excitation to the lower maser level or to any level directly excited by electron collisions is much more effective with pulsed currents (having large average electron energies) than for dc currents.

A technique for decreasing the excitation to the lower maser level by utilizing a two-region discharge was tried, but its potential for increasing the output powers from He-Ne lasers was found to be marginal because of the saturation in upper maser level population with increasing electron density. Techniques for increasing the total discharge volume without increasing the minimum uninterrupted transverse discharge dimension, such as use of a tube with internal fins, appear to have considerable promise. Increasing the average electron energy in gas lasers which do not depend on excitation by resonance transfer collisions with metastables may also produce considerably higher output powers.

TABLE OF CONTENTS

LIST OF ILLUSTRATIONS

List of Illustrations (continued)

List of Illustrations (continued)

INTRODUCTION

This program was devoted to the study of techniques for increasing the power output of gas lasers. Particular attention was given to the studies of He-Ne lasers and the basic processes occurring in the discharge tubes of such lasers. Because of the CW visible operation at 6328A, He-Ne lasers are expected to be among the most useful of the gas lasers.

In order to gain a clear picture of the role of various quantities in determining the output power of a gas laser, we now discuss a simple rate-equation theory which will exhibit the important features.

THEORY OF He-Ne LASERS

We consider a two level system connected by the maser transition, as illustrated in Fig. 1. Under time equilibrium conditions, the rates of change of population of the two levels 2 and 1 are zero and are given by the following:

$$\frac{dN_2}{dt} = 0 = -\frac{N_2}{t_2} - B\rho(N_2 - N_1) + n_2 \tag{1}$$

$$\frac{dN_1}{dt} = 0 = -\frac{N_1}{t_1} + B\rho(N_2 - N_1) + f\frac{N_2}{t_2} + n_1 \tag{2}$$

where

N_2, N_1	=	populations of states 2 and 1 respectively;
t_2, t_1	=	decay times excluding stimulated processes for states 2, 1. Any other decay process is included if it is independent of N_2, N_1;
B	=	proportionality constant for stimulated processes – related to Einstein "B" coefficient;
n_2, n_1	=	rates for all processes of excitation to states 2, 1 except those proportional to N_2, N_1;
f	=	fraction of spontaneous decay processes from state 2 which terminates at state 1;
ρ	=	photon density.

Equations (1) and (2) correspond to the Ne laser transitions reasonably well. Contributing to n_2 are resonance transfer collisions between He metastables and Ne ground state atoms, various electronic excitation processes such as inelastic collisions between electrons and Ne ground state atoms and cascade processes, all assumed to be independent of N_1 and N_2. Contributing to n_1 are principally electronic excitations processes and cascade processes. The decay times t_2, t_1 are determined in He-Ne lasers primarily by the radiative spontaneous emission times, although for unusually high pressures collision de-excitation or resonance trapping may become important. Equations (1) and (2) are typical of rate-equations in that they are independent of frequency, position, and velocity distribution.

- 2 -
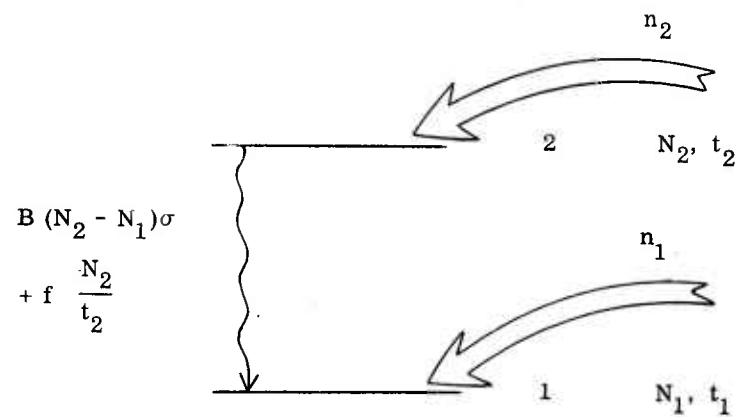
Fig. 1 - Simplified schematic of conditions and processes for a two level maser.

-3-

At oscillation conditions, the values of N_2 and N_1 are adjusted automatically so that the single pass gain equals the single pass losses, i.e.,

$$\frac{B}{c} (N_2 - N_1) = \frac{T + L}{\ell} \tag{3}$$

where

c	=	velocity of light;
T	=	fractional transmission loss of laser per pass;
L	=	fractional loss per pass excluding transmission losses;
ℓ	=	length of laser cavity.

Equation (3) holds for small values of the losses, i.e., for the case when

$$\exp(-T - L) \approx 1 - (T + L).$$

This will be true for most gas lasers utilizing high reflectivity mirrors.

Using equations (1) through (3) we can express the stimulated emission rate R in a form independent of N_1 and N_2:

$$R = B\rho (N_2 - N_1) = \frac{n_2 (t_2 - ft_1) - n_1 t_1 - \frac{C(T + L)}{B\ell}}{t_1 (1 - f) + t_2} . \tag{4}$$

In many cases $t_1 \ll t_2$, while f is always less than 1, in which case (4) can be approximated by

$$R \approx n_2 - n_1 \frac{t_1}{t_2} - \frac{C(T + L)}{B\ell\, t_2} . \tag{5}$$

Evidently, from Eq. (4) and (5), (and also intuitively evident), the stimulated emission rate can be increased by increasing the rate of excitation n_2 to level 2, by decreasing the rate of excitation n_1 to level 1, or by decreasing $\frac{t_1}{t_2}$. For $t_2 \approx t_1$, R can also be increased by decreasing f, the fraction of decays from level 2 which terminate at level 1.

- 4 -

In He-Ne lasers, it is thought that the major contribution to n_2 comes from resonance transfer collisions between He metastables and Ne ground state atoms. If such is the case, then n_2 will be approximately proportional to the He metastable density which depends on electron density as is schematically illustrated in Fig. 2. For low electron densities, the metastable density increases linearly, while for large electron densities, the metastable density saturates. This behavior can be explained by considering the various reactions that can occur in a discharge to affect the He metastable density. These reactions are the following:

(1) $He + e + 19.8\ ev \rightarrow He^m + e$

(2) $He^m + e + K.E. \rightarrow He^+ + 2e$ (or $He^* + e$)

(3) $He^m + e \rightarrow He + e + 19.8\ ev$

(4) $He^m + He^m \rightarrow He^+ + He + e$

(5) $He^m + Ne \rightarrow He + Ne^+$

(6) $He^m + 2He \rightarrow He_2^* + He.$

The superscripts are the following: m metastable, + ion, * excited state other than metastable, no superscript refers to ground state. To this list of reaction should be added the normal diffusion processes which lead to de-excitation of He metastables at the walls of the discharge tube. In a He-Ne laser using normal gas partial pressures (a few tenths to a few mm of Hg), reaction (6) will be small compared to the rest. The rate-equation for the He metastable density can then be written:

$$\frac{d\,He^m}{dt} = C_1\,He\,n - C_2\,He^m\,n - C_3\,(He^m)^2 - C_4\,He^m\,Ne + D\,\nabla^2\,He^m \qquad (6)$$

where

$C_1,\ C_2,\ C_3,\ C_4$ = proportionality constants for reaction rates

D = diffusion constant for metastables.

The various factors C_i, $i = 1, 2, 3, 4$, are velocity averages of products of cross-sections and relative velocities, and are thus dependent on velocity distributions. C_1 is the constant for reaction (1), C_2 for the reactions (2) and (3), C_3 for reaction (4) and C_4 for reaction (5).

- 5 -

Metastable
Density
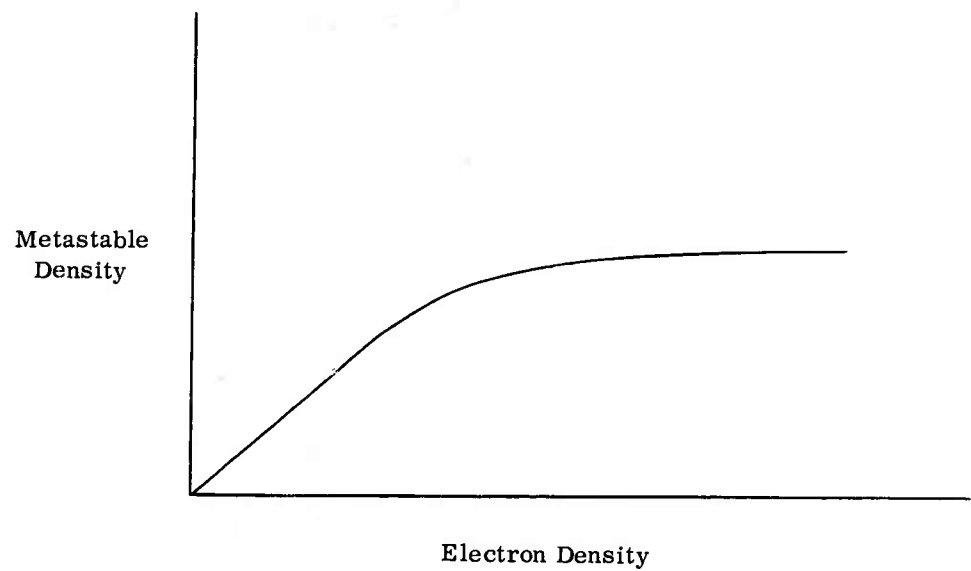
Electron Density

Fig. 2 – Schematic illustration of metastable density vs electron density
in a discharge.

-6-

Under some conditions, the last term in Eq. (6) will be small compared to some of the other terms, i.e., diffusion loss of the metastables can be neglected when compared to other losses. Then Eq. (6) can be set equal to zero for equilibrium conditions and solved algebraically for He^m. The result is

$$He^m \simeq \frac{1}{2C_3} \left\{ -(C_2 n + C_4 Ne) + \left[(C_2 n + C_4 Ne)^2 + 4C_1 C_3 He\, n \right]^{1/2} \right\}. \quad (7)$$

For small values of the quantity $\dfrac{4C_1 C_3 He\, n}{C_2 n + C_4 Ne}$, Eq. (7) reduces to

$$He^m \simeq \frac{C_1 He\, n}{C_2 n + C_4 Ne} \qquad\qquad (8)$$

and such is the case when C_3 is small, i.e., when the term $C_3 (He^m)^2$ in Eq. (6) is negligible. Equation (8) predicts a metastable density (He^m) variation like that in Fig. 2, i.e., a linear increase for small values of n, and a leveling off to a plateau at

$$He^m \approx \frac{C_1 He}{C_2}$$

for large values of n. When the C_3 term is included, it has the effect of making the transition between the linear and plateau regions in Fig. 2 less abrupt and increases the values of n necessary to reach the plateau region.

When diffusion loss for He metastables are important, Eq. (6) becomes a nonlinear differential equation which requires numerical solution and a knowledge of the electron density profile. However, it is clear that the essential dependence of He^m on n as depicted in Fig. 2 will be unaltered.

The rate of excitation n_2 to the upper maser level will be the sum of that due to resonance transfer collisions and that due to inelastic collisions between electrons and Ne atoms. The two processes have different dependences on the electron density, the first as shown in Fig. 2, the second a linear or possibly superlinear dependence on n. It is therefore possible to determine which process is more important by measuring the upper maser level population as a function of n.

Excitation to the lower maser level is caused principally by inelastic collisions between electrons and Ne atoms. For single collision processes, the rate of excitation n_1 will be a linear function of n, while cumulative excitation processes requiring two successive

electron collisions will produce a quadratic dependence on n. Cumulative excitation will take place at large values of n, while single collision excitation will predominate at small values of n. This dependence is illustrated in Fig. 3. The single collision processes include excitation from the ground state directly to level 1, as well as cascade processes involving excitation to states higher than level 1 with subsequent decays to level 1. The cumulative excitation processes will be principally those involving collision excitation from the Ne metastable or quasi-metastable 1S levels directly to the lower maser level, or to a higher level with subsequent cascading to the lower maser level. If cascading from levels which are populated by resonance transfer collisions with He metastables is important, then n_1 may show some saturation as n increases.

In general, the reaction rate for a collision process between two species A and B, each having a single fixed velocity, is given by

$$N_A \, N_B \, \sigma_{AB} \, v_{AB} \tag{9}$$

where

$$N_A, \, N_B \quad = \quad \text{particle density of each species;}$$

$$\sigma_{AB} \quad = \quad \text{cross-section for the reaction;}$$

$$v_{AB} \quad = \quad \text{magnitude of the relative velocity between A and B particles.}$$

When the species A and B each has a distribution of velocities, but σ_{AB} is independent of v_{AB}, then (9) must be replaced by

$$N_A \, N_B \, \sigma_{AB} \left(\overline{v}_A^2 \; + \; \overline{v}_B^2 \right)^{1/2} \tag{10}$$

where $\overline{v}_A$, $\overline{v}_B$ are the mean speeds for each species. If σ_{AB} depends on v_{AB}, then (10) must be replaced by a more complicated expression. This can be simplified if v_A is much larger than v_B, so the latter can be neglected such as the case where the A species are electrons and the B species are atoms. Then (10) becomes

$$N_A \, N_B \quad < \sigma_{AB} \, v_A > \tag{11}$$

where the brackets indicate the velocity average.

- 8 -
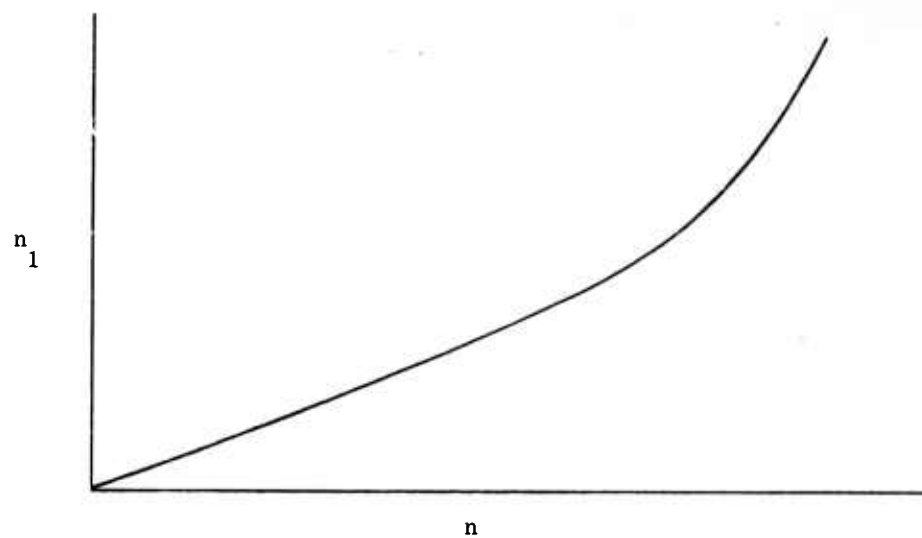
Fig. 3 - Sketch of dependence of n_1 on electron density n.

-9-

12443

For inelastic processes resulting in transfer of energy from the electron to an atom, σ_{AB} is zero below the excitation energy, rises to a maximum and then usually decreases with increasing energy, as illustrated in Fig. 4. For single-collision excitation, only the electrons with energies somewhat above the threshold energy are effective, thus, high average electron energies are important for efficient excitation of a gas. In fact, schemes for increasing the average electron energy in gas lasers are among the most promising for increasing the efficiencies or output powers.

As was shown in Eq. (5), the stimulated emission rate depends on $\dfrac{t_1}{t_2}$, the ratio of the lifetime of the lower maser level to that of the upper, and increases as this ratio decreases. In the He-Ne laser, t_2 is the radiative lifetime of the upper maser level for all transitions except those to the ground state, the rate for the latter being small because of resonance trapping of the associated radiation. The lifetime of the lower maser level t_1 is determined by radiative transitions to the 1S Ne levels. Two of these levels are metastable while the other two are effectively metastable because their radiative lifetimes are greatly lengthened due to resonance trapping. Because of their metastability, the 1S levels can become appreciably populated in discharges operated at high electron densities. When this occurs, the lifetime t_1 may also be lengthened due to resonance trapping, resulting in an additional mechanism for reduction of the stimulated emission rate and output power. As we have mentioned previously, the presence of large concentrations of Ne atoms in the 1S levels might also result in increased excitation by electron collisions to the lower maser levels, thus also decreasing the output power.

The amount by which t_1 is increased by resonance trapping can in principle be calculated from the theory of Holstein.[1] The effective lifetime t_e is given in a cylindrical discharge tube by

$$t_e = t \; \frac{k_o R \; (\pi \log k_o R)^{1/2}}{1.60} \tag{12}$$

where k_o is the absorption coefficient at the center of the Doppler broadened line t is the untrapped lifetime, and R is the radius of the discharge tube. The expression for k_o is

$$k_o = \frac{N \lambda_o^3}{8 \pi^{3/2}} \; \frac{g_2}{g_1} \; \left(\frac{M}{2kT}\right)^{1/2} \; \frac{1}{t} \tag{13}$$

- 10 -
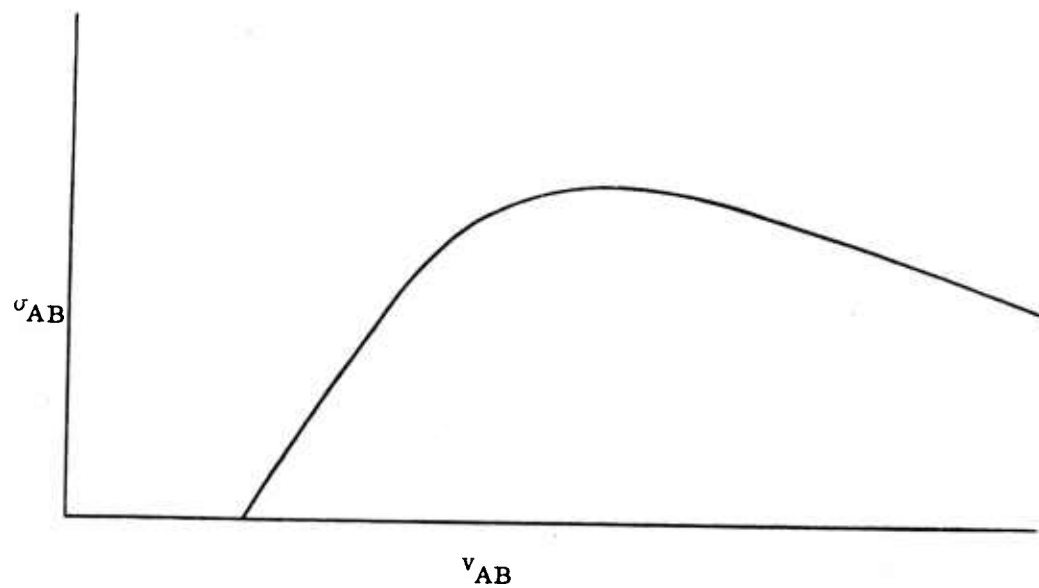
Fig. 4 - Illustration of behavior of excitation cross-section with relative particle velocity.

-11-

where

N $\quad = \quad$ number of atoms in the lower level of the transition

$\lambda_o \quad = \quad$ wavelength at center of line

$g_2, g_1 \quad = \quad$ statistical weights of upper and lower states, respectively

M $\quad = \quad$ atomic weight

t $\quad = \quad$ natural lifetime for the transition.

Figure 5 contains sketches showing both n_2 and $n_1 \dfrac{t_1}{t_2} + \dfrac{C(T+L)}{B\ell\ t_2}$ as a function of n for two cases of interest. According to Eq. (5) the difference between curve (a) and (b) or (c) is proportional to the stimulated power. If it were possible to depress curves (b) and (c), then the stimulated power would be increased. It is clear however, that if curve (c) fits the He-Ne laser, then depression of that curve will produce only moderate increases in the stimulated power. However, if curve (b) is appropriate, then quite significant power increases might be achieved by a depression in that curve. The essential difference between the two situations is whether the plateau in curve (a) is reached at smaller or larger values of n than that at the intersection of the curves. Experiments were conducted during this program in order to determine the shapes of the n_1 and n_2 curves and these will be discussed later.

A useful technique for measuring the power output potential of a laser is that of single-pass gain measurement under conditions of negligible stimulated emission. It is easily shown from Eqs. (1) through (4) that, if α is the non-regenerative gain constant for a gas laser defined by

$$P(x) \quad = \quad P_o e^{\alpha x}$$

where $P(x)$ is the power density at a point x and P_o is the power density at a starting point, then the stimulated power density p is such a laser under oscillation conditions is given by

$$p \quad = \quad \frac{C\ \alpha\ell\ -\ (T+L)}{B\ell\ t_1\ (1-f) + t_2} \tag{14}$$

This expression is good enough for our purposes - a more accurate description would take into account the spontaneous emission line shape and the cavity mode widths, and would yield an expression not exactly linear in $\alpha\ell$.[1] The stimulated power is thus directly proportional to the single-pass gain minus the single-pass loss in a laser.

- 12 -
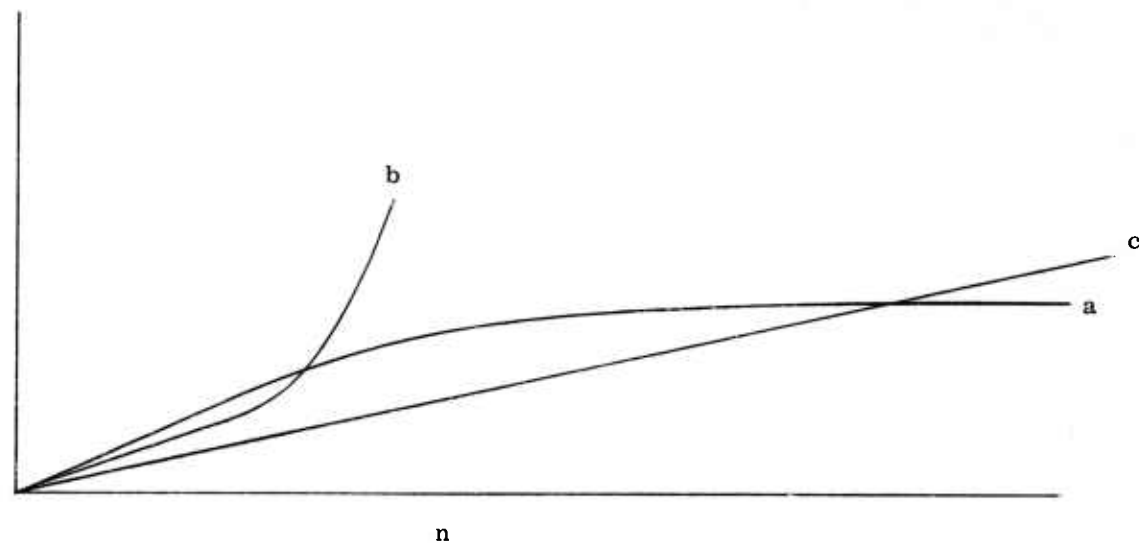
Fig. 5 - Sketches of (a) n_2 and (b, c) $n_1 \dfrac{t_1}{t_2} + \dfrac{C\,(T+L)}{B\ell}\,t_2$ as functions of n for two different cases.

-13-

HIGH POWER GAS LASER TECHNIQUES

Several techniques for achieving high powers from gas lasers were considered during the earlier phases of this program. The techniques considered can be separated into two classes, those employing constricted discharge techniques, and those utilizing a separation of the laser into two regions.

Constricted Discharge Techniques

It is well known that the single-pass gain of a gas laser increases as the discharge tube diameter decreases, at least down to diameters of a mm or two.[2] This gain increase is a result of the increase in density of atoms in any excited state providing the discharge parameters approximate those for similarity relations to hold. Two discharge tubes are said to be similar when all of the dimensions of one are scaled by a single constant (a) from the other, voltages and currents are the same in both, and the gas pressures are inversely proportional to the scaling constant (a). Then under equilibrium conditions, the density of atoms in an excited state which decays radiatively is inversely proportional to a^3 and the density of atoms in a metastable state is inversely proportional to a^2. These relations are easily shown as follows.[3]

Under equilibrium conditions the density of excited atoms N^* obeys the following relation, when decay is primarily by radiative transitions:

$$C_1 \, nN - \frac{N^*}{t} = 0$$

where

n = electron density

N = ground state atom density

t = lifetime of excited state

C_1 = proportionality constant

and we have assumed that the principle process for excitation of the atoms is by collisions between electrons and ground state atoms. For similar discharges[3]

$$N \propto \frac{1}{a}$$

$$n \propto \frac{1}{a^2}$$

- 14 -

so

$$\frac{N^*}{t} \propto \frac{1}{a^3} \qquad (t = \text{constant}) \tag{15}$$

However, when atoms are de-excited primarily by collisions with walls, then t is no longer independent of a, but becomes proportional to a. This arises because the rate of diffusion to the walls is proportional to $\frac{D}{a^2}$ and

$$D \propto \frac{1}{N} \propto a.$$

In this case,

$$N^* \propto \frac{1}{a^2} \qquad (\text{metastables}). \tag{16}$$

For states which have t dependent on (a) in an intermediate way between being constant and being proportional to (a) N^* will be inversely proportional to a power of (a) between 2 and 3. Such will be the case for states which decay radiatively but with a large probability of reabsorption before the photon leaves the tube (resonance trapping). Relations (15) and (16) will hold for values of (a) large enough so that collision processes are not important in determining t. For smaller values of (a), N^* may saturate and become independent of a.

This discussion can be applied to gas lasers albeit only in a qualitative manner[4] because gas laser discharges which are adjusted for maximum laser output do not precisely obey the similarity laws. Experiments at Watkins-Johnson confirm that the laser gain of a discharge tube does increase inversely with the tube diameter, but for optimum output powers, the tubes do not precisely obey the scaling laws for similar discharges. It is found that the gas pressure for maximum output power may vary more slowly with scaling factor (a) than as $\frac{1}{a}$. Measurements elsewhere[2] also indicate that the inverse gain is proportional to (a) rather than a higher power of (a) as would be indicated by (15) and (16). This deviation from the similarity laws may be a result of the presence of production and decay processes for the excited states other than those discussed above.

Since the gain of a laser tube increases as the diameter decreases, one technique for increasing the output power of a laser is to construct the discharge in such a manner that the cross-sectional area is large but the distance from any point in the discharge to a wall is small. One method of accomplishing this would be to use a laser tube with

- 15 -

many small tubes or rods, as shown in Fig. 6. Laser action could occur in the interstices and tube interiors. Such a geometry would require plane parallel rather than spherical mirrors, and some means of coupling the many lasing filaments together would be necessary so that the output would be coherent. Besides the coupling problem, there exists the problem of maintaining discharges simultaneously along many paths. Because of the nonlinearity of the resistances presented to the power source by the discharge paths, each path must be isolated electrically from each other one in some manner. These problems perhaps can be alleviated somewhat by utilizing a finned discharge tube as shown in Fig. 7. With this type of tube, it will even be possible to use spherical mirrors if a mode with azimuthal symmetry is used. We have done no experimental work in this program on such types of discharge tubes.

Two-Region Gas Lasers

As was discussed above, one of the primary reasons for saturation of power output in a He-Ne gas laser is excitation to the Ne 2p terminal laser level by inelastic collisions between electrons and the Ne 1s metastables or ground state atoms, and by cascade processes. Thus, one method of reducing the saturation phenomenon, and thereby increasing the possible output powers, is to reduce the contact between Ne atoms and the discharge electrons. This can be done by separating the laser into two regions, excitation of He to the ^3S (or ^1S) metastable states occurring in the first region, and resonant transfer of energy from the He to the Ne with subsequent laser action occurring in the second region. The electron discharge is confined to the first region so that cumulative excitation to the Ne 2s levels cannot occur in the second, emissive, region. This technique is expected to be most effective for the excitation curve of Fig. 5b. We now discuss techniques for accomplishing the separation of discharge region from emission region.

Confinement by Grids

The most practical means of separating the laser into two regions appeared to be by the use of a grid which presented a sheath barrier to discharge electrons, but which was porous enough to allow substantial transmission of the metastable atoms. A practical geometrical arrangement of such a grid is shown in Fig. 8.

A positive ion sheath forms at any surface in contact with the discharge plasma. The wall potential, i.e., the potential at the surface, is negative with respect to the plasma potential and the potential increases rapidly away from the surface. The sheath thickness is approximately one Debye length L, where

$$h = \left(\frac{kT}{4\pi ne^2} \right)^{1/2} = 6.90 \left(\frac{T}{n} \right)^{1/2}$$

- 16 -
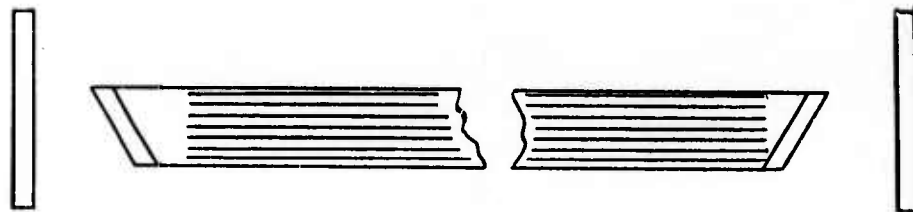
Fig. 6a - Laser using many internal tubes or rods,
Brewster angle windows, and plane parallel mirrors.
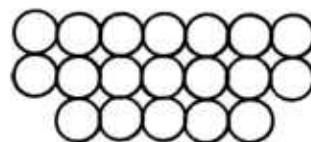
Fig. 6b - Enlarged end view showing loose packed array
of quartz rods. Laser action would occur in the interstices.
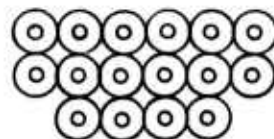
Fig. 6c - Enlarged end view showing loose packed array
of quartz tubes. Laser action occurs both in the interstices
and in the tube interiors.

-17-

11148
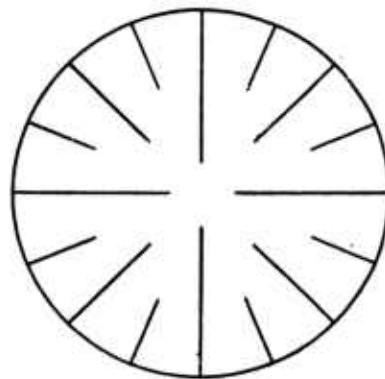
Fig. 7 - Finned discharge tube with azimuthal symmetry for producing
a constricted discharge.
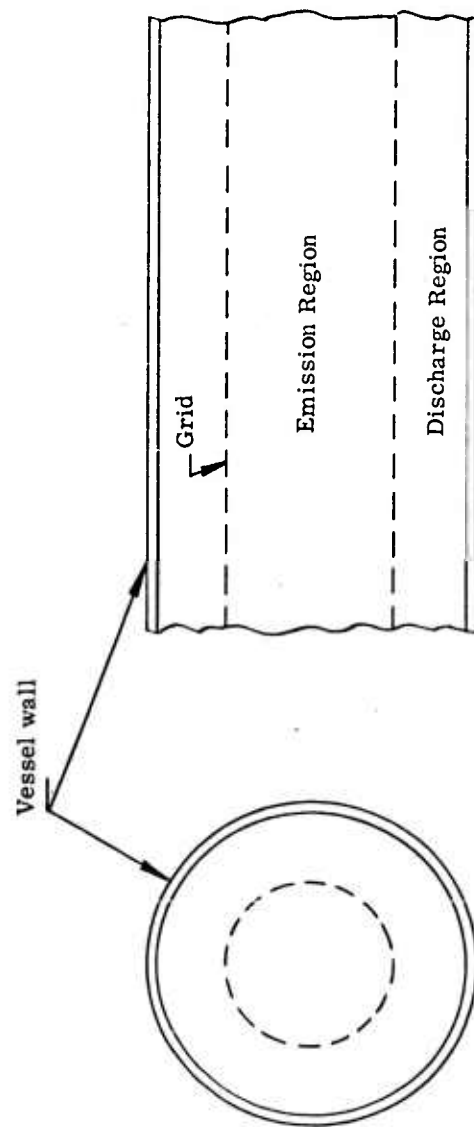
Fig. 8 – Geometry of gridded two-region discharge tube.

Vessel wall

Grid

Emission Region

Discharge Region

- 19 -

(c.g.s. units) where

- k = Boltzman's constant
- T = electron temperature
- n = electron density
- e = electronic charge.

The potential distribution in a sheath is illustrated in Fig. 9. The spacing between wires in the grid should be roughly one Debye length or less in order for the grid to present a solid potential barrier to the electrons. No bias need be applied to the grid to confine the electrons because the natural formation of the sheath provides an automatic bias.

Excitation of the gas mixture occurs in the discharge region. The majority of the electrons are confined to the discharge region by the sheath potential barrier at the grid. The electrically neutral components including He metastables, are free to diffuse through the grid spacings into the emission region.

Detailed Analysis of Gridded Two-Region Discharge Tubes

We now discuss in more detail, the characteristics of the emission region of a two-region laser. We assume the geometry of our gridded tube, i.e., a discharge in an outer annular region and laser action in the central region, as shown in Fig. 8. The concentration of He metastables is also shown schematically in the figure. We shall concern ourselves with the details of only the central, emission region, for $r \leq R_1$. In this region the following diffusion equation applies:

$$D \nabla^2 H - HN < \sigma_{HN} v > = 0 \tag{17}$$

where

- D = diffusion constant for He metastables
- H = concentration of He metastables
- N = concentration of Ne ground state atoms
- σ_{HN} = cross-section for excitation to the Ne upper maser level by collision with a He metastable
- v = relative velocity of He metastable and Ne ground state atoms.
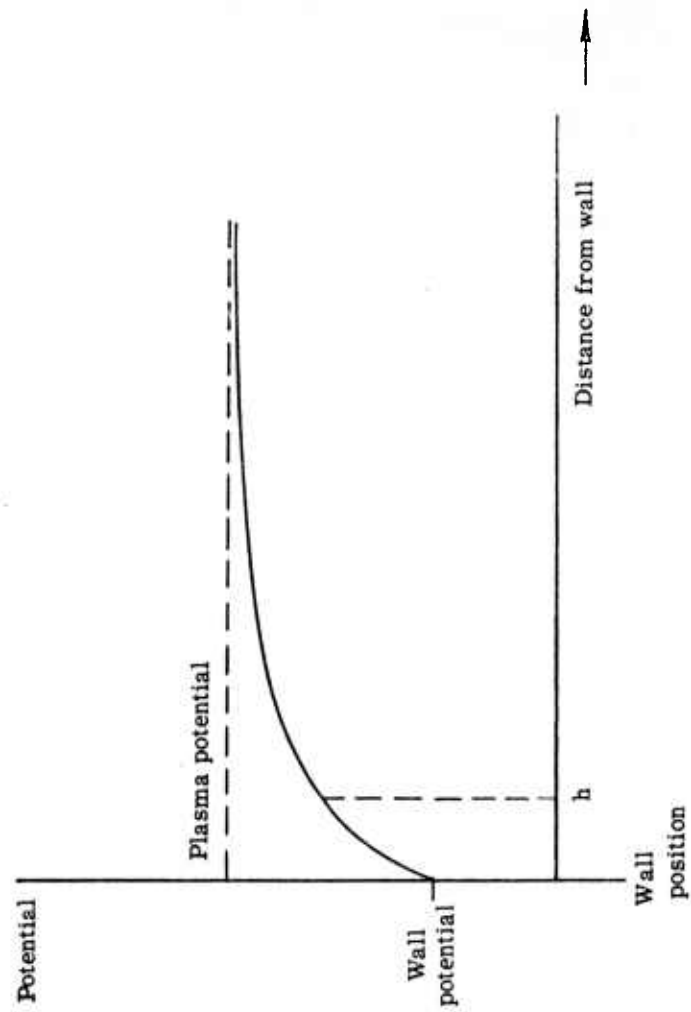
Fig. 9 – Sketch of potential distribution in a sheath.

-21-

10929

The brackets in the second term indicate an average of the produce over all velocities. Terms neglected here are contributions by He metastable-metastable ionizing collisions, He metastable-Ne metastable ionizing collisions, and effects of residual electrons in the emission region. The first and last of these may be significant in some cases and will be discussed later. The second is not expected to be important because of the relatively small density of Ne 1s atoms.

For cylindrical symmetry, the solution of Equation (17) is

$$H = H_o I_o \left(\left[\frac{N}{D} < \sigma_{HN} v > \right]^{1/2} r \right)$$ (18)

where H_o is the density at the radius $r = 0$.

In Equation (18), I_o is a hyperbolic Bessel function of the first kind or zeroth order which behaves much like an exponential. In order to calculate the variation in He metastable density (and thus Ne upper maser level density) across the inner region, the values of D and $N < \sigma_{NN} v >$ are needed. The first is known only for He ^{3}S metastables[2] (470 cm^2/sec for 1 torr pressure) but the latter is known for both ^{3}S and ^{1}S metastables[2] in contact with Ne (1.6 x 10^5 P_{Ne} and 17 x 10^5 P_{Ne} sec^{-1} respectively, where P_{Ne} is the Ne partial pressure in torr). If we assume that the value of D is the same for both ^{3}S and ^{1}S metastables, that the total pressure is 1 torr, that R_1 = 0.32 cm (corresponding to our design described below), then the ratio of the value of the He metastable concentration on the axis to that at the grid is 0.43 for the following cases:

He ^{3}S metastable, Ne pressure of 0.1 torr

He ^{1}S metastable, Ne pressure of 0.01 torr.

Design and Construction of Gridded Tube

The diameter of the grid was chosen as a compromise between minimizing the variation in excitation density over the cross-section and maximizing the total active volume. The mesh size of the grid was chosen to be comparable with the Debye length in a plasma containing an electron concentration n of 10^{11} to 10^{12} cm^{-3} and an electron temperature T about 10^5 deg K. Thus, the diameter was 0.25 in. and the grid hole diameter was 0.0035 in.

Because of the low resistance presented by the discharge, the grid was also designed for low electrical resistance. The purpose of the shorting bar spot-welded to the grid

in Fig. 11 was to reduce the grid's electrical resistance to a value less than that of the discharge. The grid was about 42 cm long, leading to a calculated discharge impedance of about 1/2 ohm, and a grid resistance (with a shorting bar 1/16 inch diameter) of about 1/5 ohm. A longer grid than this would lower the discharge impedance and raise the grid resistance so that too large a fraction of the rf power would be dissipated in the grid.

Two gridded discharge tubes were assembled. Similar techniques were used on both tubes but some details were changed in the second one. Both grids were made from flat molybdenum mesh sheets, 6 inches by 0.8 inch. The mesh was photoetched from solid stock and contained holes 0.0035 inch on a side and wires 0.001 inch in diameter.

For the first tube, the grid was constructed in the following manner: Three 6 inches long pieces of mesh were rolled up end-to-end on a 0.25 inch diameter aluminum mandrel and spot-welded into an 18 in. long cylinder using platinum ribbon as a bonding agent. The aluminum mandrel was then removed by etching. A 0.60 inch diameter molybdenum rod was then spot-welded along the seam of the cylindrical grid, again using platinum ribbon. (Figure 10 is a photograph of a grid section which has been fabricated in this manner.) The grid was then placed on a molybdenum mandrel and fired. Quartz spacers were used to support it in a glass envelope.

This method of grid fabrication was unsatisfactory because of the difficulty of spot-welding the rod to the 18 in. long grid cylinder. The second grid was constructed by spot-welding the 0.60 inch diameter rod to the flat mesh sheet first and then rolling it up into a cylinder.

When a gas discharge was run in the first tube, it was found that small imperfections in the grid, such as wrinkles, or holes, led to electric field concentrations of sufficient magnitude to develop a tiny arc at each imperfection. These arcs would produce sputtering of the grid material and lead to the development of a hole large enough for the arc to extend into the central region. The first grid had several of these imperfections, and holes in the grid large enough to make the tube unuseable soon developed. The second grid is a considerable improvement in this respect, but it also is developing a hole at the side of an imperfect spot-weld.

The fabrication of grids by spot-welding is not the ideal technique because of the tendency of the spot-welder to leave small breaks and holes in the mesh, with these imperfections subsequently becoming the sites of localized arcs when discharge is excited. More satisfactory results might be obtained by brazing. However, spot-welding is so much faster and simpler that, for the purpose of making experimental tubes, it can be satisfactory enough provided enough care is used in the fabrication.

Figure 11 is a photograph of a portion of the second discharge tube made, showing the grid and two of the seals used to bring connections outside of the glass envelope. In this tube a 0.60 inch diameter molybdenum rod runs the length of the discharge region just inside the envelope. This rod was intended as a reference electrode so that an

- 23 -
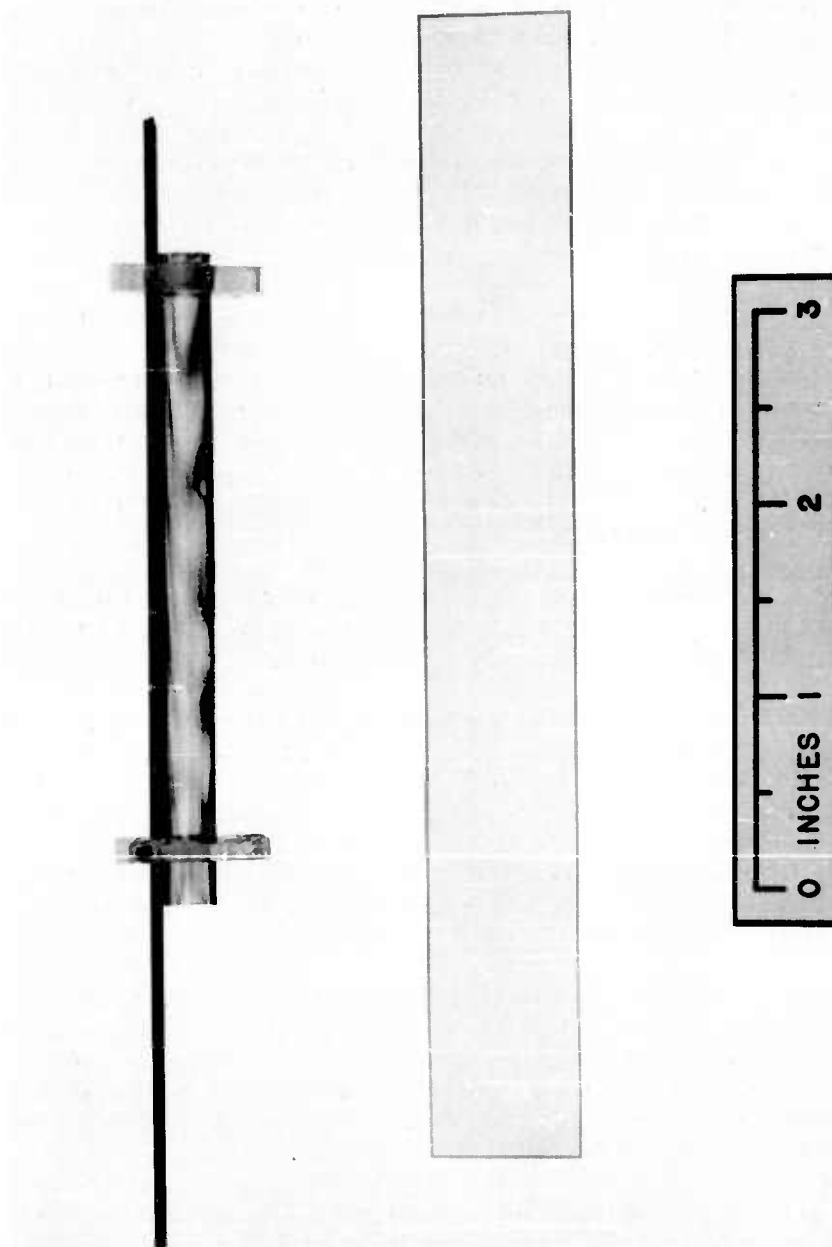
Fig. 10 – Photograph showing a completed section of cylindrical grid (top) including shorting bar and quartz spacers. This section is shorter than those actually used in the tubes. Also shown (bottom) is a section of grid material before it is fabricated into a cylinder.

- 24 -
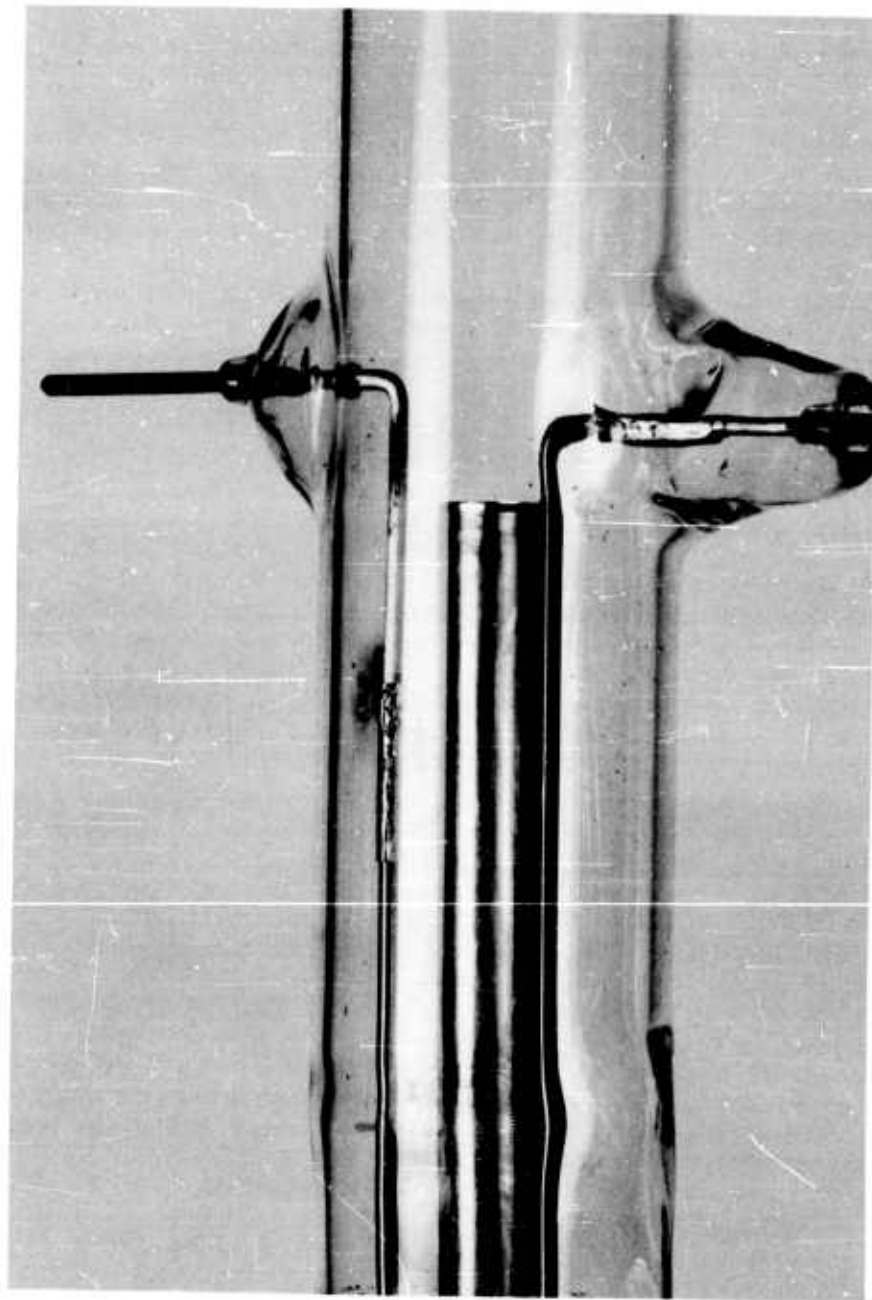
Fig. 11 – Photograph of a portion of the second tube made showing details of the feed-throughs leading to the grid and reference electrode.

arbitrary dc bias could be applied to the grid, thus controlling the concentration of electrons inside the grid. Figure 12 is a photograph of the complete tube.

This tube was not designed to be used in a laser oscillator, hence the end windows are perpendicular to the axis instead of being at the Brewster's angle. This causes no disadvantages, since the measurement of single-pass gain under non-oscillation conditions determines the output power when the laser is oscillating.

Figures 13 and 14 are photographs of the second gridded discharge tube in operation. Figure 14 is an end view revealing the difference between the light intensities in the discharge regions and inside the grid. With rf input powers of a few tens of watts, the visible light emerging from inside of the grid was much less intense than that from the discharge. This is a rough indication that much of the neon excitation, even in the presence of He metastables, arose from electron collisions with Ne atoms.

Preliminary Instrumentation of Single-Pass Gain Measurements

The experimental gridded tubes were operated in an arrangement as depicted in Fig. 15, where an rf-excited laser oscillator with a beam diameter of about 1 cm served as a signal source. The beam from one end of the signal source was used as a reference beam, while the beam from the other end was used as a sampling beam, being passed through the gridded tube. While the reference beam was not affected by changes in transmission in the sampling region, the amplitude of the sampling beam exhibited attenuation or gain after having been passed through the gridded tube.

Reference beam and sampling beam were fed into a Cary Model 14 double beam spectrophotometer, and the simplified optical and electrical operations in the tube and associated instrumentation are also sketched in Fig. 15. First the beams were chopped and alternately fed into the single optical path of the photometer, passing a monochromator which served as an effective bandpass filter. The optical signal rendered a time-division multiplex type pulse-train for the lead-sulfide cell used as a detector. Synchronizing pulses for the chopper-amplifier permit splitting into two electrical paths, which were fed into integrating networks and compared electrically with respect to their amplitudes. The accuracy claimed for this process, 0.1 percent, resulted in the maximum sensitivity of the instrument around unity absorbance. The accuracy in the zero absorbance region, which was of primary importance for our applications where we anticipated small amounts of absorption, was considerably lower, and was estimated to be approximately one percent.

- 26 -
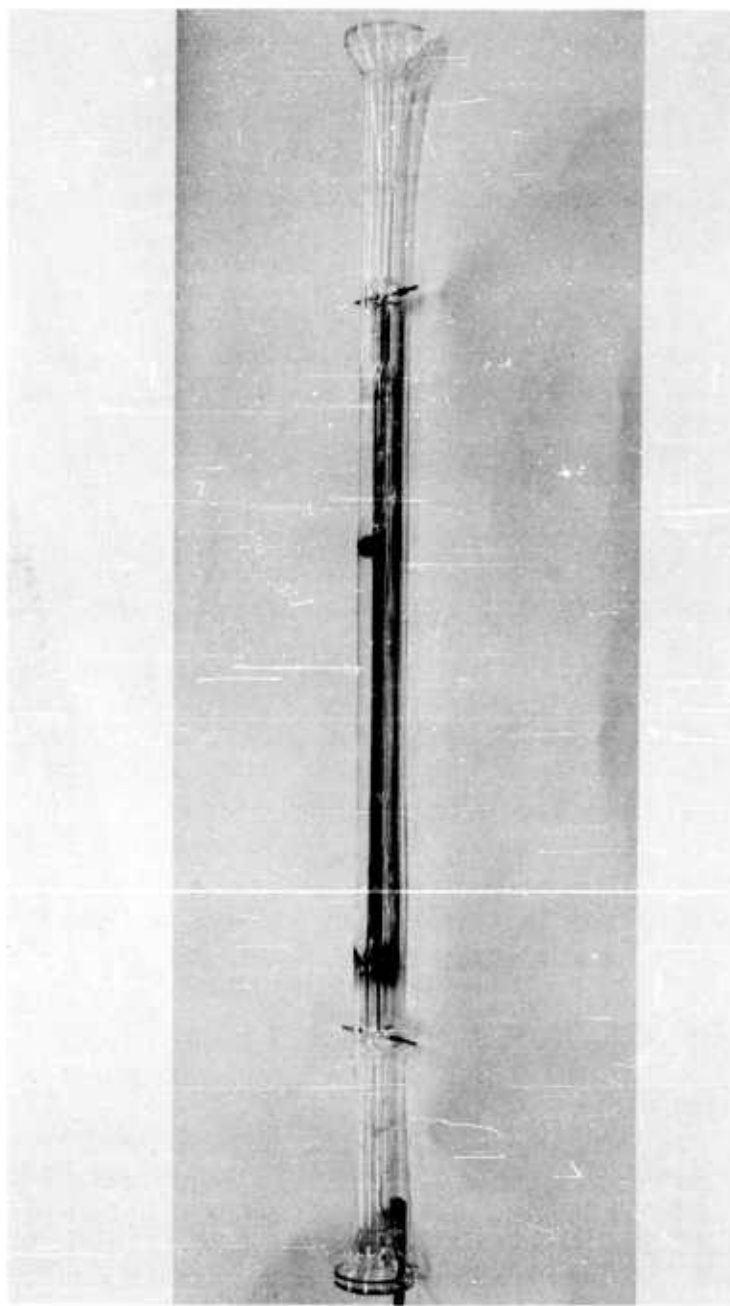
Fig. 12 - Photograph of discharge tube No. 2.
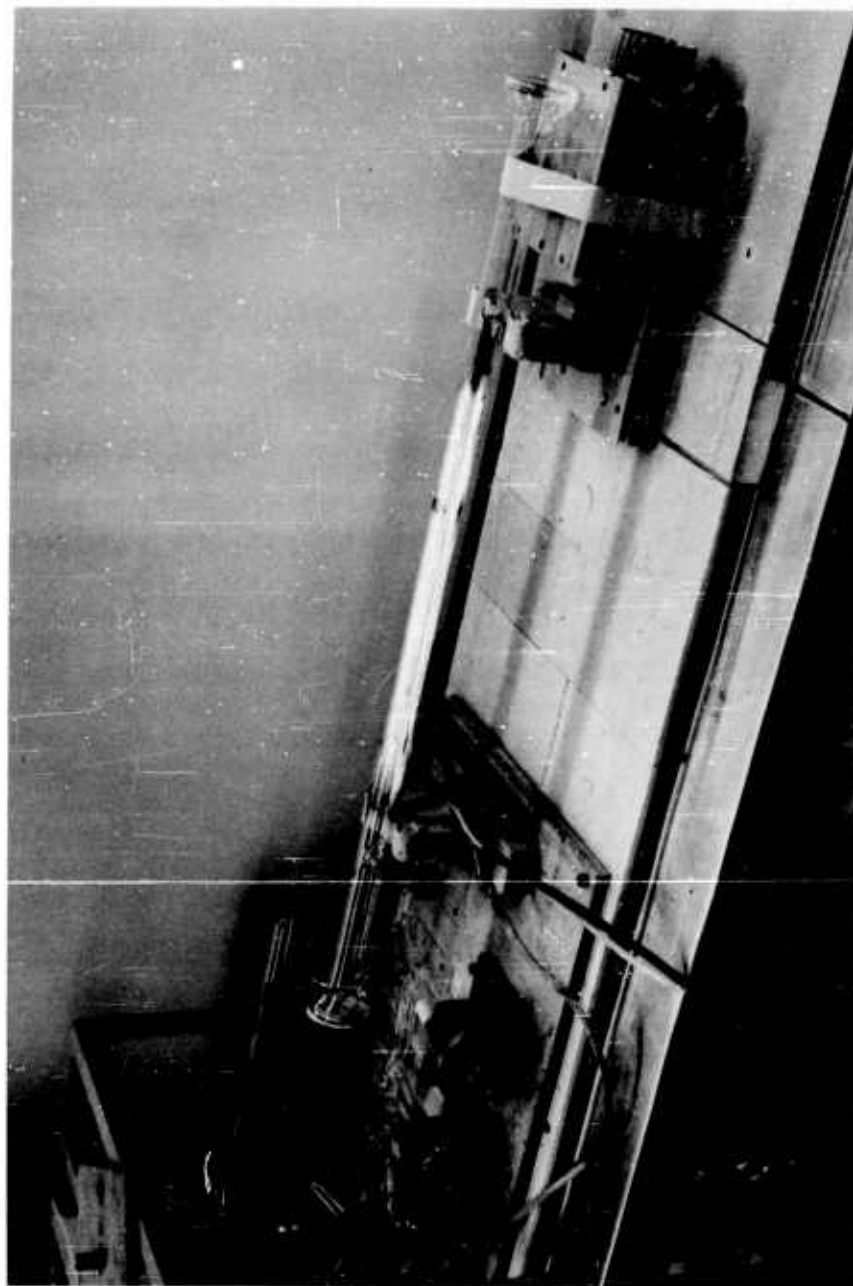
Fig. 13 - Photograph of the gridded discharge tube in operation. The rf voltage is applied between the grid and an external rod running along the far side of the tube.

Fig. 14 – Close up end view of discharge tube in operation. The region inside the grid (central dark area) is considerably less emissive in the visible than the region outside.
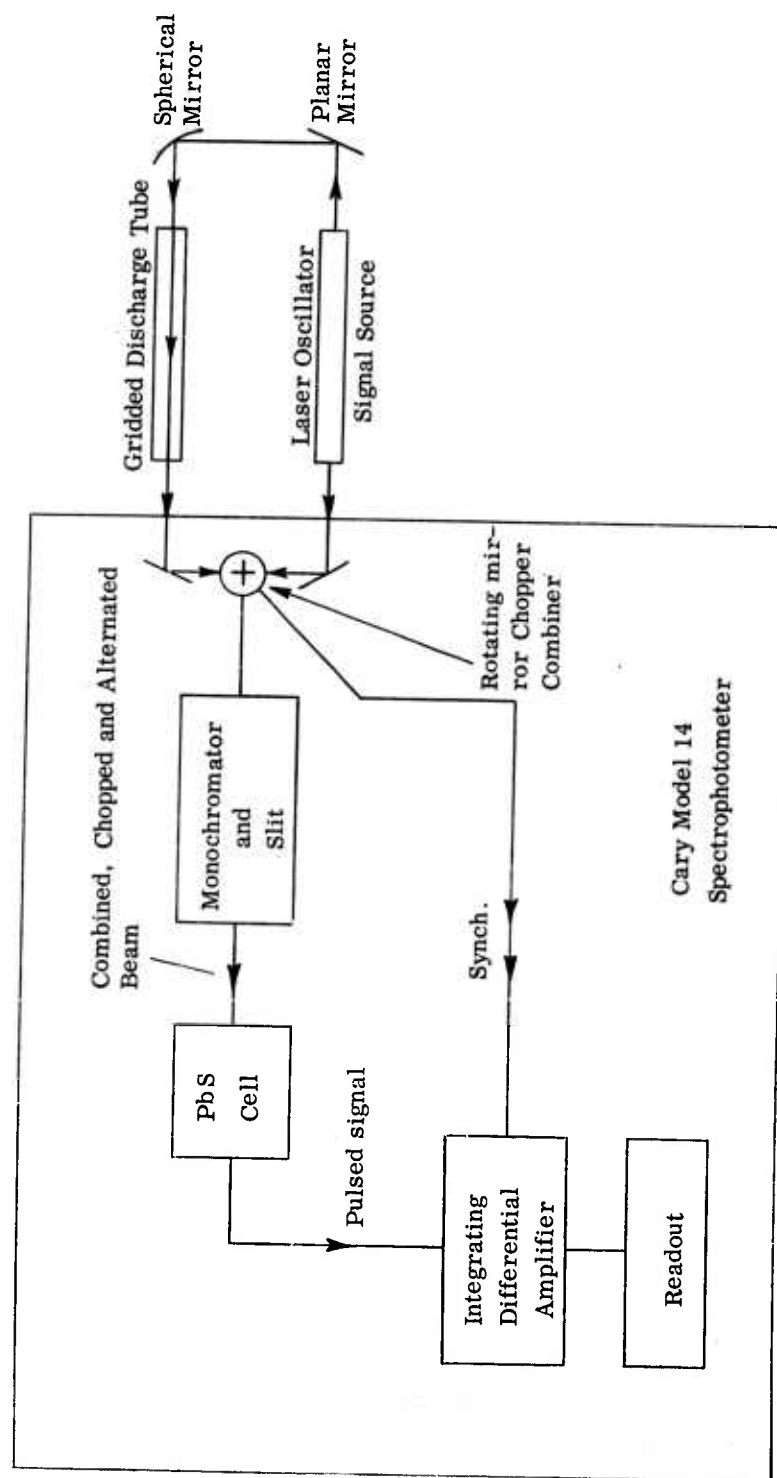
Fig. 15 - Experimental arrangement to determine single-pass gain in the gridded tube.

11938

Final Instrumentation of the Single-Pass Gain Measurements

After it had become apparent that the sensitivity of the arrangement of Fig. 15 was insufficient to produce conclusive results, the following measurement scheme was devised and realized physically in the laboratory.

The method used is shown in Fig. 16. It only differs from that of Fig. 15 in the method of detection and readout, and in the fact that a more stable, higher output power and more sharply collimated reference as well as sampling beam was used. This was possible through utilization of the WJ-270 dc pumped laser which produces a small diameter beam with high stability and power.

As in the arrangement shown in Fig. 15, reference and sampling beams are passed into the detector circuit, which now is represented by a dual chopper, two photocells and a differential amplifier plus oscilloscope.

Single-Pass Gain Measurements on the Cary Spectrophotometer

Using the arrangement shown in Fig. 15, the ratio of the intensities of reference and sampling beam was determined. This procedure was performed for the discharge in the gridded tube on and off, and the gain in the gridded tube then was specified by the ratio of the two numbers obtained. The minimum gain that could be measured was determined by the characteristics of the spectrophotometer and largely limited by equipment resolution such as detector noise and integration properties, as well as the optics of the beam paths, mechanical vibration in the apparatus, and noise in the test oscillator. The sensitivity of this apparatus was about one percent.

Modulation of the gridded discharge tube together with phase sensitive detection were not used because the sensitivity of the much simpler system described above was judged adequate for the specific purpose.

Measurements were made at $1.15\,\mu$ wavelength for signal paths both inside the grid and outside the grid in the discharge region, according to the following table.

He (torr)	Ne (torr)	Gain Inside Grid	Outside Grid
0.4	0.1	0	0
0.9	0.1	0	0
5.9	0.1	0	0
0.8	0.2	0	0
1.4	0.4	0	1 percent
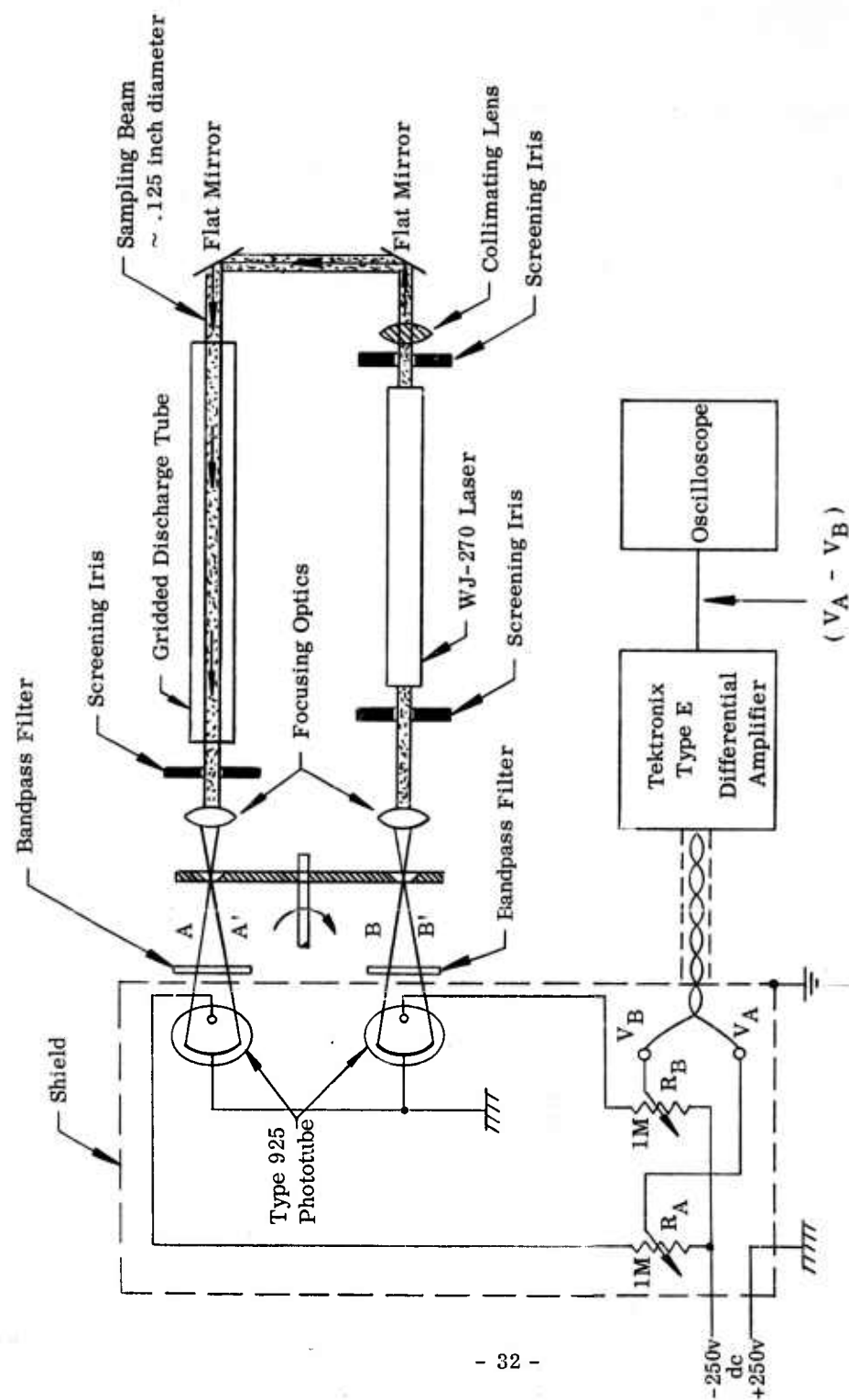
Fig. 16 – Small gain or absorption measurement arrangement using dual beam techniques.

- 32 -

11939

Positive gain was measured for only one condition - - at the latter pressure and for a path outside the grid in the discharge region.

The absence of gain on the inside of the grid in the above measurements is not surprising in view of the fact that little or no gain was observed outside the grid. In the case where 1 percent gain was measured outside the grid, the gain inside was expected to be smaller, and probably undetectable with our apparatus. The reason is that the rf power input, which was a few tens of watts, was less than the value needed for saturation of gain outside the grid and under these conditions, maximum gain is expected where the largest density of He metastables exist, namely in the discharge region between the grid and the wall of the tube.

To increase the sensitivity of the measurement apparatus, the arrangement of Fig. 16 was resorted to and a more powerful rf excitation source was installed to produce the discharge excitation densities judged necessary for conclusive measurements. The single-pass gain measurements were done at the visible 6328A wavelength, using the WJ-270 laser as a signal source.

Single-Pass Gain Measurements on the Refined Measurement Setup

The new measurement apparatus yielded minimum detectable gains of about 0.15 percent. Under these conditions it turned out that the minimum detectable signal coincided with the values of gain predicted for the relatively short length of the gridded tubes, of the general magnitude of .1 percent. Although larger values were predicted for the $1.15\,\mu$ wavelength, measurements could not be carried out on a refined setup, due to lack of time and funds remaining. This was mainly caused by the fact that the experience gained on the $6328\AA$ setup, where the experimentor literally can see what he is doing, cautioned us against attempting measurements with unsufficiently refined components. These would have to have been purchased for this purpose. The results of the gain measurements at $6328\AA$ are plotted in graph form in Figs. 17 and 18.

Considering the fact that the noise level was of the same order or larger than the useful signal, one can appreciate that the measurement readings have to be taken with the greatest care. They are meaningful principally because the signals were displayed on an oscilloscope so that a good deal of the noise could be visibly distinguished from the desired signal.

The very low values of the measured gain indicated that the proposed mechanism of operation for the two-region laser was faulty. The next section describes some measurements which were made to clarify the situation and which explain the low gains measured.
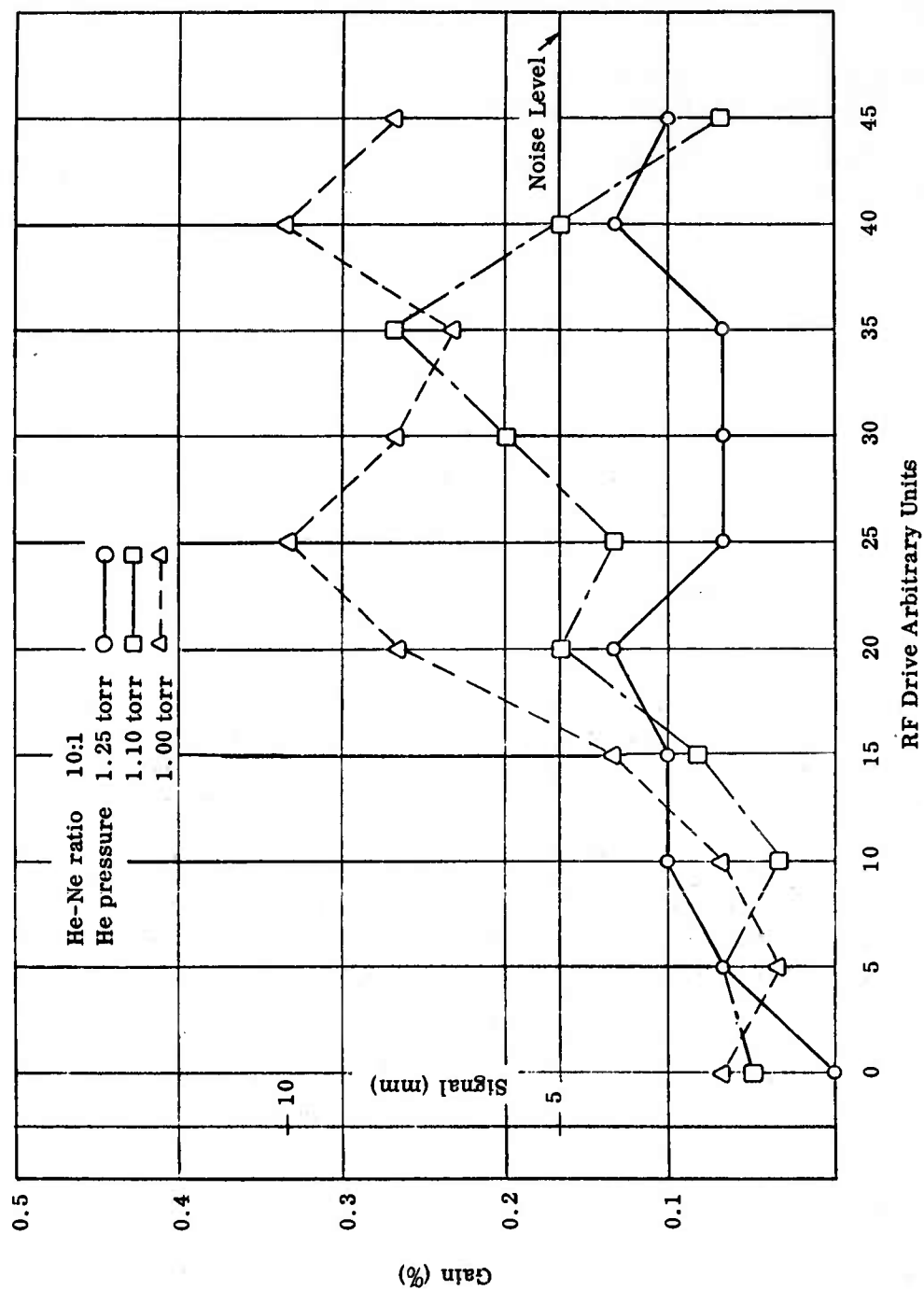
Fig. 17.- Single-pass gain inside grid.

- 34 -
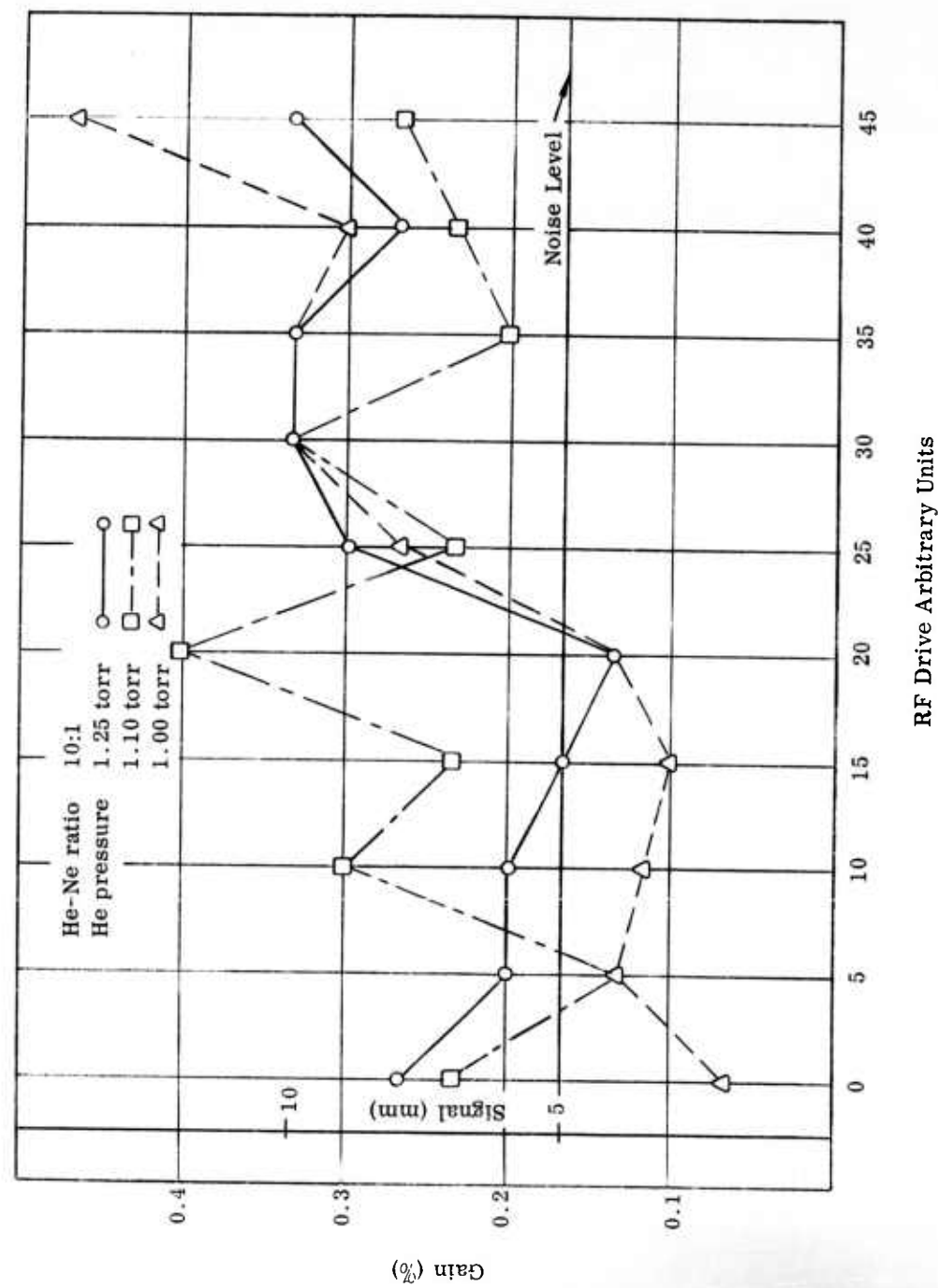
Fig. 18 – Single-pass gain outside grid.

11941

MEASUREMENTS OF BASIC PROCESSES IN He-Ne LASERS

In order to understand the reasons for the low gain present in the two-region discharge tube and to provide additional information about the basic mechanisms operating in He-Ne lasers, a program to measure the spontaneous and stimulated emission output for several transitions was conducted. For this purpose, the discharge tube from a WJ-283 gas laser was used. This tube was a dc discharge tube, with a discharge path length of 17 cm and an I.D. of .15 cm, with a heated oxide-coated cathode, and filled with a 6:1 ratio of He to Ne at a total pressure of 1.9 torr.

Measurements were made of the light emitted from the side of the tube at $6328Å$ and $5945Å$, the latter wavelength corresponding to the $2p_4 \rightarrow 1S_5$ transition as shown in Fig. 19. Measurements were also made of the laser output powers at 1.15μ and $6328Å$, all as functions of the discharge current.

For a dc discharge tube operated in the constant voltage region of the V-I characteristic as in these experiments, the electron density is proportional to the current[5, 6] and the average electron energy is independent of current. Thus, the dc measurements can be interpreted in terms of electron density as well as current.

Besides the dc measurements, measurements were also made using a pulsed current, with a pulse length of 5 μsec, superimposed on a dc current. The dc current was used to maintain a discharge between pulses so that the high voltages necessary for breakdown at each pulse were not needed. The electrical circuit used is illustrated in Fig. 20.

The V-I characteristics, both for the dc and the pulsed voltages and with a stabilizing resistor of 50 K, are shown in Fig. 21. The keep-alive current for the pulsed measurements was 5 ma. The voltage is only that across the discharge tube, not including the stabilizing resistor. It is seen that the dc characteristic is normal for a tube of this type, the voltage being nearly constant over a wide range of currents. However the pulsed characteristic is distinctly different, and represents a fixed positive resistance of about 430 K. This difference between the two characteristics can be explained if the time required to develop substantial further ionization is greater than the pulse length, so that only the keep-alive electron density is present during the course of the pulse. In this case, the resistance of the discharge during the pulse is given merely by the initial electron concentration and collision frequency. As is seen in Fig. 21, however, the pulsed current curve does not pass through the 5 ma point of the dc current curve, indicating that either the full electron density is not available to carry the pulse current, or that perhaps the formation of a sheath at the cathode results in a substantial fraction

3.39 μ

20.6 $2\,{}^{1}S$ ——— $3S_2$

20.3 $3p_4$

19.8 $2\,{}^{3}S$ ——— $2S_2$

$6328\overset{o}{A}$ $1.15\,\mu$

18.7 $2p_4$

$5945\,A^{o}$

16.6 $1S_5$

Energy
(ev)

He   Ne
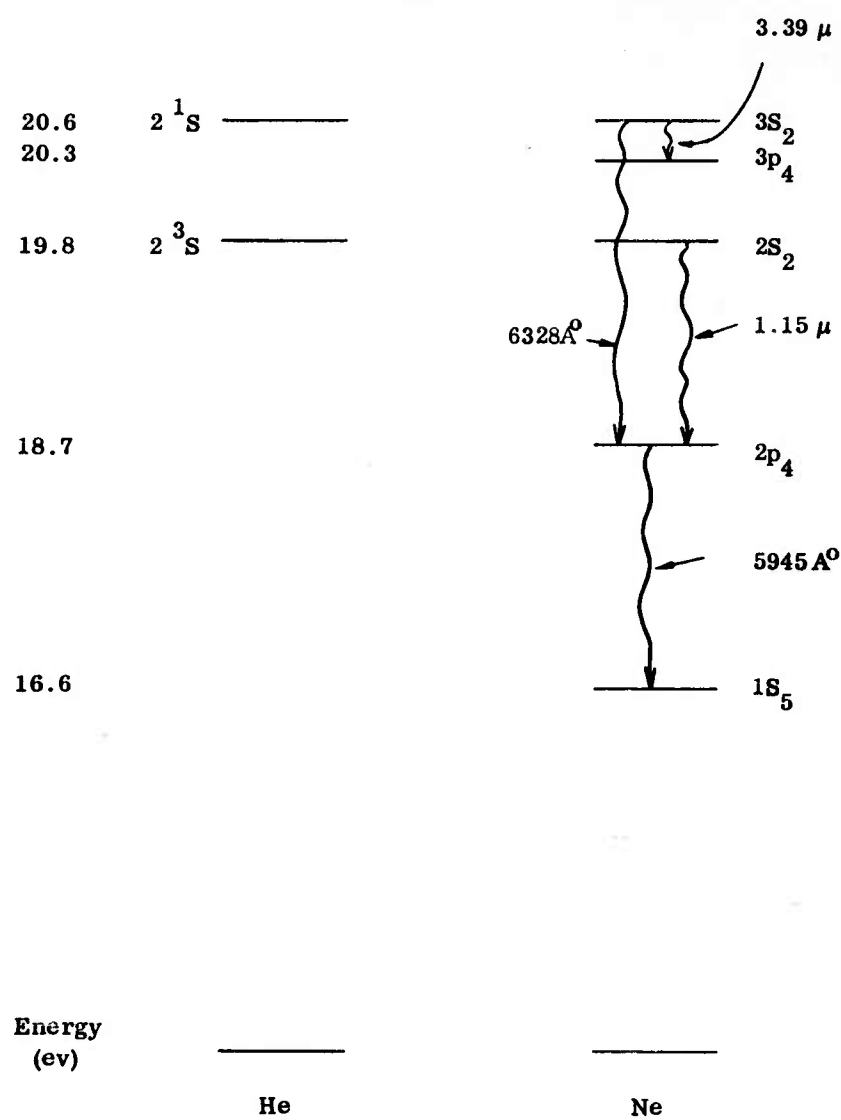
Fig. 19 - Energy levels and laser transitions for
He and Ne.

-37-
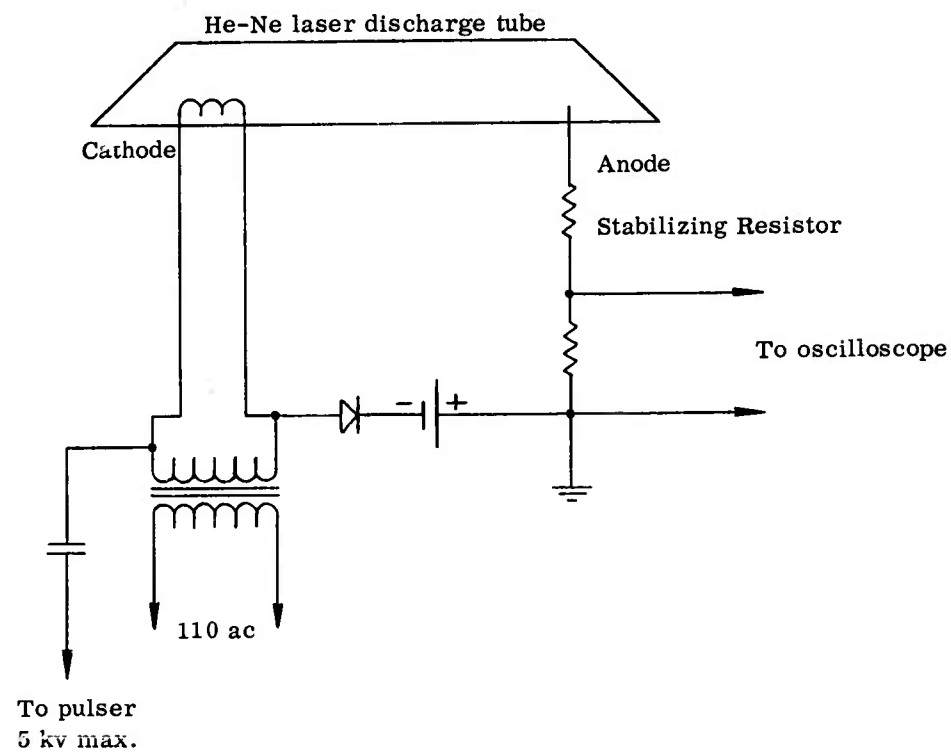
Fig. 20 - Schematic drawing of pulsing and keep-alive circuit for laser tube.
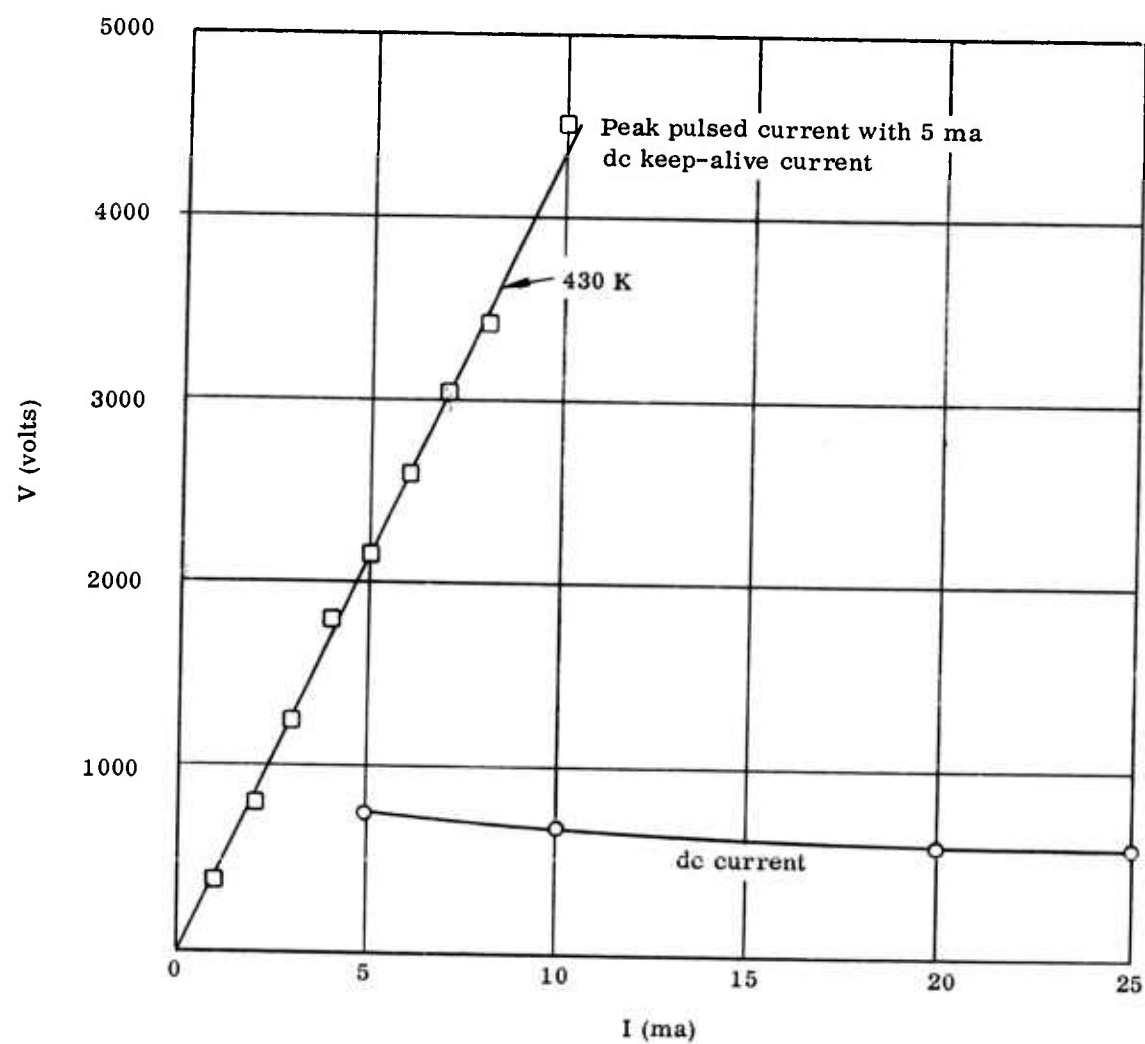
Fig. 21 - V-I characteristics for laser tube.

- 39 -

of the voltage being dropped in that region. The true reason is not yet known. In any case, during the pulse the average energy of the electrons is almost certainly increased because the increased electric field in the positive column increases the drift velocity. Much of the increase in average energy will result in larger random velocities of the electrons because the time needed to redistribute the energy is less than the pulse length. This thermalization time t_T is given by

$$t_T \;=\; \frac{M}{2M} \; t_c$$

where

m   =   electron mass

M   =   atomic mass

t_c =   electron collision time.

In our experimental tube t_T is about 0.8 μsec which is considerably less than the 5 μsec pulse length.

The spontaneous emission measurements were made with the aid of a Cary Model 14 grating spectrophotometer and photomultiplier detectors. For the pulsed measurements, the electronic time constant of the photomultiplier output circuitry was always less than 2 μsec. The laser output power was also measured with a photomultiplier at the same time that the spontaneous measurements were made.

Figure 22 summarizes the measurements made under dc conditions for the $3S_2 \rightarrow 2p_4$ and the $2p_4 \rightarrow 1S_5$ transitions, at 6328Å and 5945Å, respectively. While the spontaneous emission measurements were made while the laser was oscillating, a change of only a few percent was observed when the oscillations were prevented by placing an obstruction in the laser cavity, thus the curves also represent the non-lasing condition.

The curve labeled $3S_2$ represents the 6328Å side light - it exhibits the saturation effect for large discharge currents that was discussed earlier. The presence of the saturation indicates that the principle mechanism contributing to excitation to the $3S_2$ level is resonance transfer from He 's metastables.

The curve labeled $2p_4$ represents the 5945Å side light. This curve is also slightly convex upward instead of being linear or even superlinear, as would be expected from Fig. 3. The curvature indicates that a significant source of excitation to the $2p_4$ level
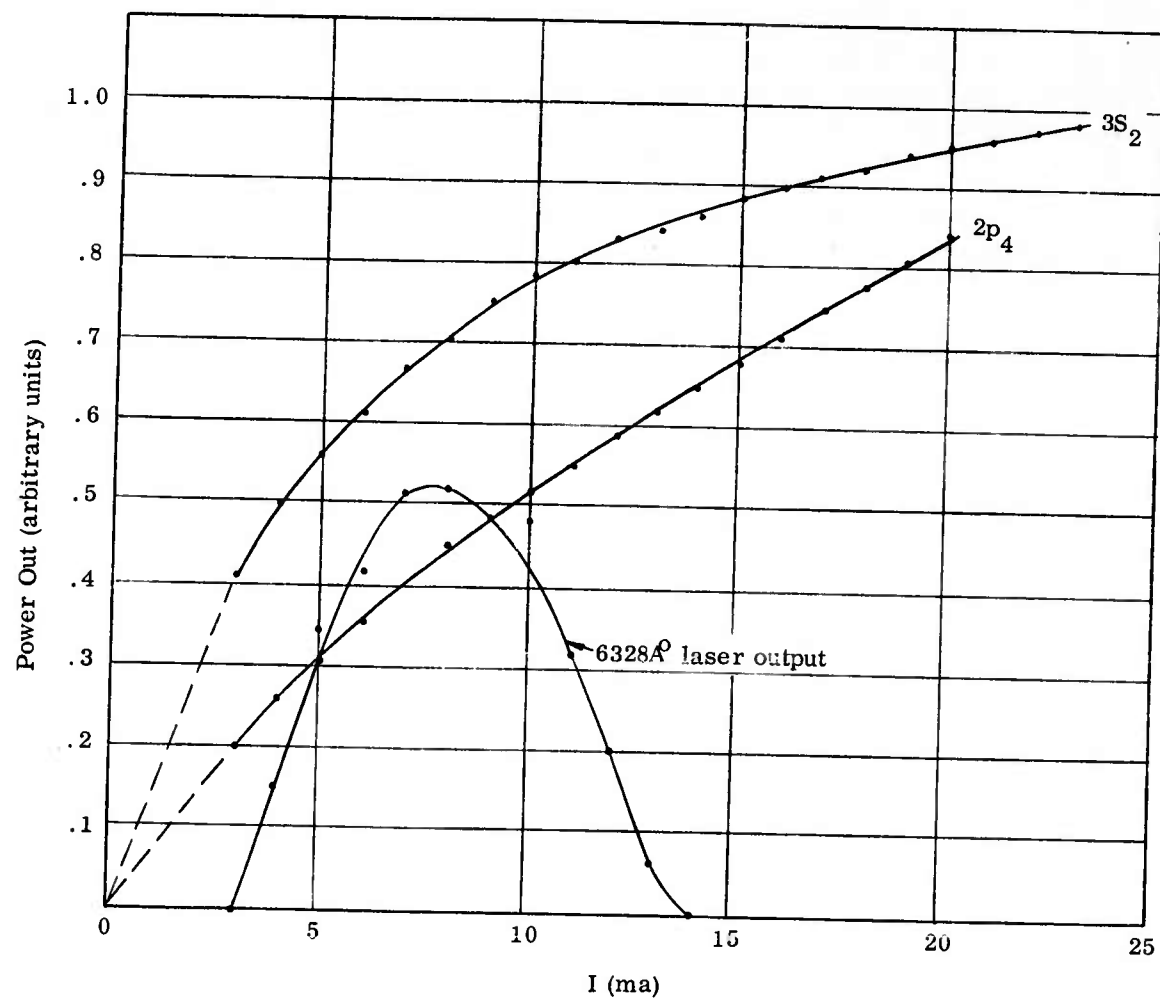
Fig. 22 - Results of power output measurements. The curve labeled
$3S_2$ is the sidelight at 6328Å, that labeled $2p_4$ is the sidelight at 5945 Å,
and the third curve is the laser output.

12450

is due to cascading from the $3S_2$ level or other levels whose population saturates with increasing discharge current. Another reason for the curvature may be the onset of resonance trapping of the $5945\text{\AA}$ radiation because of an increase in the population of the 1S levels, although there exists evidence to the contrary.[7] The $2p_4$ curve has been scaled in such a manner that for the two currents (3 ma and 14 ma) at which the $6328\text{\AA}$ laser output curve drops to zero, the differences between the $3S_2$ and the $2p_4$ curves are equal. This scaling technique will position the $3S_2$ and $2p_4$ curves properly with respect to each other, and the two curves will represent the actual populations in the two respective levels (assuming that resonance trapping does not affect the lifetime of the $2p_4$ level). The population difference between the upper and the lower maser levels must be the same for zero net gain both at the high and low ends of the laser output curve.

It is clear now that the $2p_4$ curve is closer to case (b) of Fig. 5 than to case (a). This means that the gains in the center region of the two-region discharge tube described previously are probably only a factor of two or three greater than the gain in the outside region (where the gain is expected to behave as Fig. 22 indicates). This explains the lack of large gain in the measurements at $6328\text{\AA}$ on the two-region discharge tube.

Pulsed measurements were made of the spontaneous emission (side light) output at $6328\text{\AA}$ and $5945\text{\AA}$, and of the laser output at $6328\text{\AA}$ and $1.15\,\mu$. These measurements were made with a repitition rate of 60 pps and peak currents of from zero to 50 ma.

Figure 23 shows photographs of the results of the pulsed laser output measurements at $6328\text{\AA}$ for three different values of the peak pulsed current, 0.2, 0.5 and 1.0 ma, and for a dc keep-alive current of 5 ma. Each photo contains two oscilloscope traces, the upper is the pulsed discharge current (current increases negatively), and the lower is the laser output as measured with a photomultiplier.

In all of the photos, time increases towards the left (output increases negatively). In the first photo, with 0.2 ma peak pulsed current, the laser output increases during the current pulse. In the second photo with 0.5 ma peak current, the output decreases during the current pulse (the oscillation inthroughout apparently is caused by the over-shoot spike on the leading edge of the current pulse). In the third photo, with 1.0 ma peak current, the laser output rapidly decreases to zero at the beginning of the pulse and remains there until the pulsed current dies to a small value. Only in the first photo was the laser output increased by the current pulse. It is very striking that laser action could be completely stopped with a peak current of less than 1 ma, while it was necessary to increase the dc current from 5 ma to about 14 ma (see Fig. 22) before oscillations ceased. The results at $1.15\,\mu$ are similar to those described above.

- 42 -
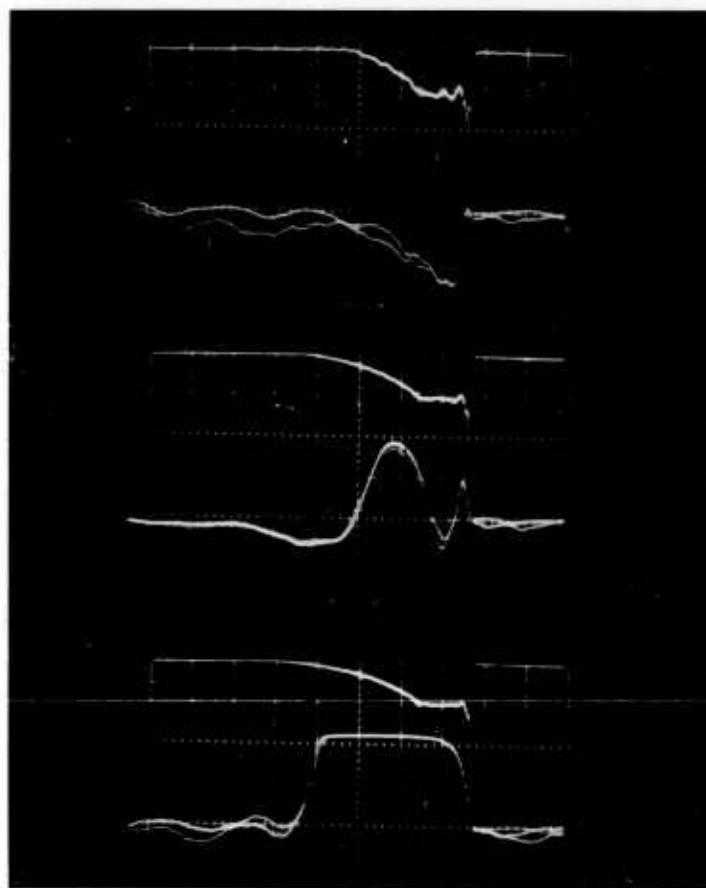
Fig. 23 - Photograph of oscilloscope traces of pulsed discharge currents and laser outputs at 6328Å. In each of the three photos, the current is given in the top trace, laser output in the bottom, both increasing downward. Horizontal scale increases toward left, 5 μsec per large division. Current traces are given by 0.2, 0.5, and 1.0 ma per large division, respectively. Trace sensitivity of laser output is the same in all three photos.

This remarkable behavior is partially explained by the results of the side light measurements at 5945Å, as shown in Fig. 24. The variation of power out as a function of discharge current is plotted and the curves represent the lower maser level population. It is seen, that for small currents, the slope of the pulsed current curve is about 8 or 10 times greater than the dc curve (but the slope of the pulsed curve approaches that of the dc curve at higher currents). Thus, for small currents, the pulsed current is an order of magnitude more effective at populating the lower maser level than is the dc current.

Measurements were also made of the pulsed behavior of the 6328Å side light for dc keep-alive currents of about 5 ma. These measurements were less accurate because of the small light intensities, but they indicated that there was little or no additional population contributed to the upper maser level by the pulsed current. (Obivously there must be a small amount of enhancement in order to explain the first photo in Fig. 23; however, this small amount could not be detected in the side light measurements.) These results are to be expected if the upper maser level is populated principally by resonance transfer collisions from He metastables, and the metastable density is near the saturation value. The higher average electron energies during the pulses are not likely to result in large changes in the saturation values of metastable densities from those for dc currents.

Since there is little change in the upper maser population and a large increase in lower maser level population during a pulse, maser action is inhibited or stopped, and the results of Fig. 23 are explained. These results have considerable significance with respect to techniques for increasing the output powers from gas lasers. They indicate that, for a laser depending on excitation by resonance transfer collision from a met - stable population whose density is at or near its maximum during normal dc operation, little or nothing will be gained by schemes to increase the average electron energy. On the other hand, for lasers depending on excitation to the upper maser levels by direct electron excitation, the peak output powers may be considerably increased by using techniques for increasing the average electron energy.
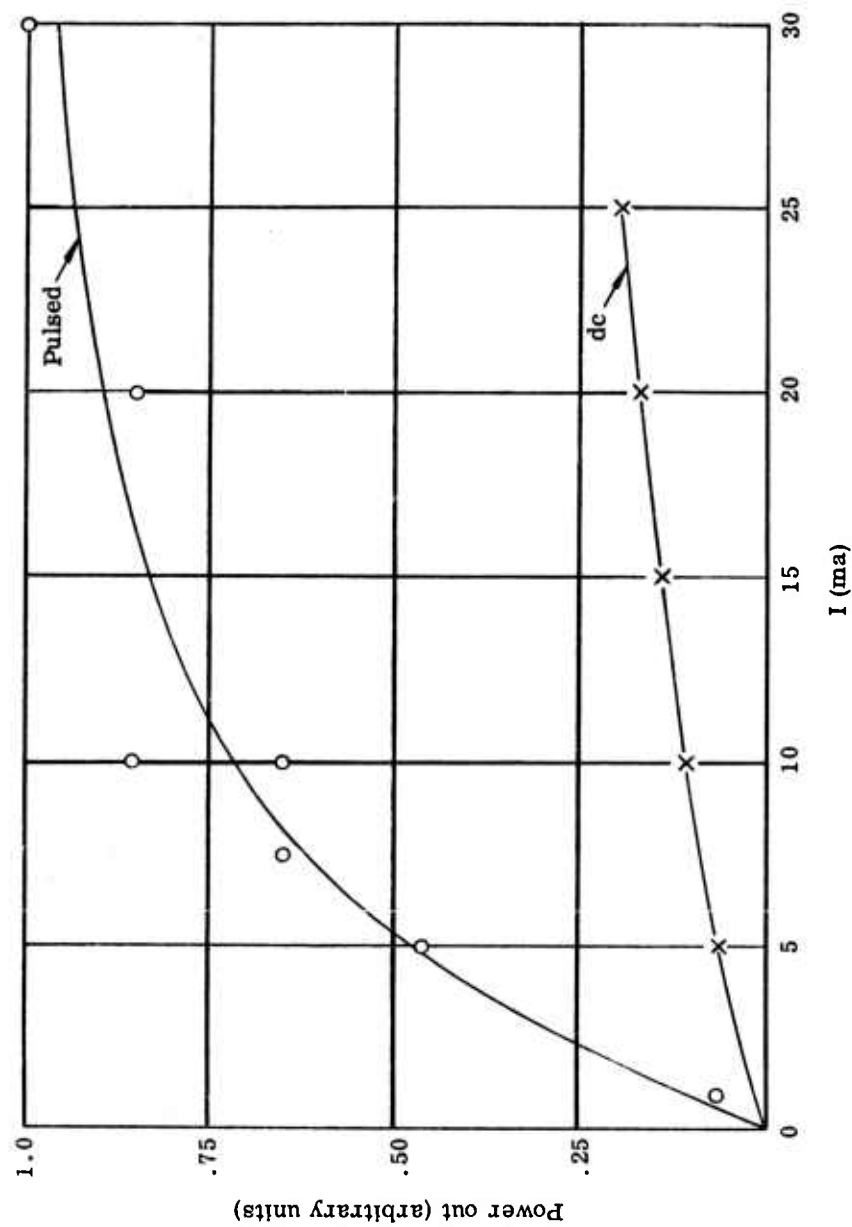
Fig. 24 - Spontaneous emission at 5945Å for both dc and pulsed currents. The pulse length was ~ 5 μsec and the keep-alive current was 5 ma.

12451

CONCLUSIONS

The principle mechanism for excitation to the Ne $3S_2$ upper maser level in the He-Ne laser is resonance transfer collisions between He metastables and Ne ground state atoms. The principle mechanism for excitation to the $2p_4$ lower maser level is inelastic collisions between electrons and ground state Ne atoms, and cascade processes. The output power of ordinary He-Ne lasers operating at 6328Å and 3.39 μ is limited by the saturation in population of the $3S_2$ level with increasing electron density. Any scheme for increasing the output powers at 6328Å and 3.39 μ must include techniques for increasing the saturation value of the $3S_2$ density. One apparently feasible scheme is the one of decreasing the effective transverse dimensions of the discharge tube while increasing the volume, such as the use of a discharge tube with internal fins which lie along model planes of the optical cavity modes.

Pulsing a discharge results in order of magnitude increases in the effectiveness of excitation to a level by electron-atom collisions. The increased effectiveness is apparently a result of the high average electron energies during a pulse. Schemes for increasing the average electron energies may considerably increase the efficiency of gas lasers although the output power may not increase if the laser normally operates in a region where the upper maser level population is nearly independent of electron energy as is the case with the He-Ne laser operating at 3.39 μ and 6328Å. On the other hand, lasers which depend on direct electron-atom collision excitation to the upper maser level, such as all gas lasers except the He-Ne type, may benefit by techniques to increase the average electron energy because population of the upper, as well as the lower, maser level may be increased by these techniques.

He-Ne lasers which depend on the separation of the discharge into two regions in order to reduce the electron density in an emission region (such as the scheme described in this report) may offer only slight power increases because they do not solve the basic problem of increasing the population in the upper maser level.

- 46 -

REFERENCES

1.   T. Holstein, "Imprisonment of Resonance Radiation in Gases". II,Phys. Rev. $\underline{83}$, 1159 (1951).

2.   See the review by W. R. Bennett, Jr., Applied Optics Supplement on Optical Masers, 1962, p. 24 ff.

3.   See, for example, Gordon Francis, Ionization Pehnomena in Gases, (Butterworth Scientific Publications, London, 1960) Chapter 3.

4.   E. I. Gordon and A. D. White, private communication.

5.   S. C. Brown, Basic Data of Plasma Physics, (Technology Press of MIT and John Wiley and Sons, N.Y., 1959), Chapter 14.

6.   E. F. Labuda and E. I. Gordon, private communication.

7.   A. D. White and E. I. Gordon, private communication.

APPENDIX I

DESCRIPTION OF THE WATKINS-JOHNSON LASER TUBE
PROCESSING AND FILLING STATION

The exhaust and filling station described centers around a 2" diameter EIMAC oil diffusion pump, and provides a large degree of flexibility in operation. The complete station is shown in Fig. 8 of the Interim Engineering Report No. 1, of 15 August 1962, on Contract AF 33(657)-8986. A block diagram of the station is shown in the attached sketch, Fig. 25.

Mechanical roughing pump, oil diffusion pump and liquid nitrogen cold-trap are standard commercial components. So are the thermocouple and ionization gauge of Fig. 25, as well as the instruments to read these gauges. All items are marked and called out in the enclosed copy of the referenced Engineering Report.

The station is supported by a stable frame welded from sections of 1.5" angle-iron. Manifolds and valves are mounted on top of a 1" thick masonite sheet, which serves both as mechanical support as well as for heat isolation. Metal borders permit sliding of the bakeout-hood (a double walled masonite filled and cal-rod equipped box, with the bottom and the front face missing) over either the processing base, or over the manifold-valve support base. Bakeout temperatures of 450°C are feasible with the arrangement, due to the use of hard glass for manifolds and vacuum lines. The valves can only be baked in the open position, and tube lines 1 and 2 have to be tipped off prior to bakeout.

Let us now go through the entire processing and filling cycle, for a typical laser tube, to give a practical operating procedure of the system. The tube is to be connected to Line 1, which has been tipped off on a previous occasion and is being pumped from the manifold. Flask Valves are closed, Pump Valve is open, Tube Valves 1 and 2 are open.

First, Pump Valve 1 is closed by means of the torque wrench, to approximately 25 foot-pounds. The diffusion pump is shut off, and permitted to cool, to prevent cracking of the oil by the air which is to be admitted to the system. Tube Line 1 is opened and the tube is connected. With the diffusion pump off and cold, a fore-pump vacuum is pulled in the tube by opening of Tube Valve 1. The glass is checked for leaks with a Tesla coil. The diffusion pump is switched on, after leakchecking. This will produce an increase in pressure at first, noticed on the Thermocouple Gauge as well as on the Pirani Vacuum Gauge in Positions 1, 2 or 3. After zero reading of the Pirani Gauge has been
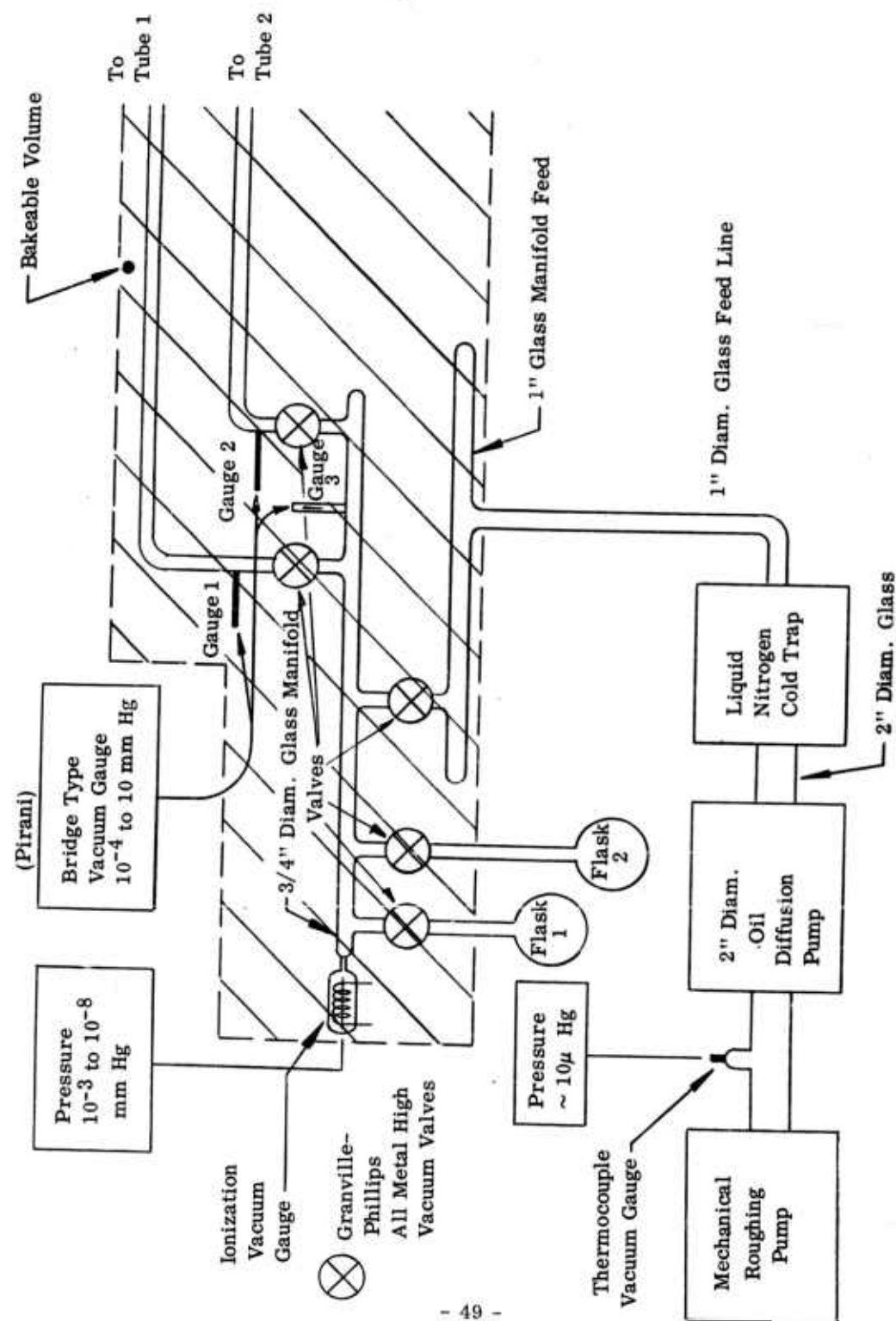
Fig. 25 – Basic layout of the processing and filling station.

12186

accomplished, the Ionization Gauge supply is switched on, and a vacuum of 10^{-4} mm can normally be read after approximately 30 minutes.

The bakeout-hood is placed over the tube, shielded at its open front with aluminum foil and the thermocouple temperature control is set to the desired bakeout temperature. The temperature can also be raised over a fixed period of time, usually by 100°C per hour in critical cases where thermal shock is to be avoided.

For tubes producing large amounts of gas during bakeout, it is recommended to leave the diffusion pump off until the system pressure has dropped to $10 \times 20 \times 10^{-3}$ mm Hg, to avoid contamination of the hot oil. For specific processing information, see "Tube Laboratory Manual", Research Laboratory of Electronics, Massachusetts Institute of Technology.

Close to the completion of bakeout and exhaust, the cold trap is filled with liquid nitrogen, and the oven is normally shut off when no further decrease in pressure occurs with time. After cooling to 100°C, the hood is lifted off, and filling can begin.

The station provides for two types of gas to be connected to the gas valves, the gas being contained in one liter glass flasks. Once the tube and system has cooled to room temperature, the pump valve is closed off.

The pressure will rise in the manifold to a value determined by the characteristic of the system, but normally on the 10^{-5} scale. If higher pressures are found and the pressure increases, a leak is indicated which is located by squirting acetone on inspected areas, with the tube pumping and by watching for bursts on the ionization gauge readout.

With the pump valve closed tightly, the gas valves are carefully opened and, varying the conductance of the valves, pressure is observed on the Pirani Gauge. Using the calibration curves supplied with the gauge, the desired gas mixtures are readily obtained, whereupon the gas valves are closed tightly. After filling, a time of 15 minutes should be allowed for mixing of the gas. Then, with Tube Valve 1 closed, the tube is tipped off. If the tip-off is found tight (Pirani gauge), Tube Valve 1 and the Pump Valve are opened, and the station is ready for the next cycle.

APPENDIX II

STABILIZATION AND AMPLITUDE MODULATION OF THE
DISCHARGE IN A DC-PUMPED HELIUM-NEON GAS LASER TUBE

Stabilization of an arc-discharge of the type used in dc-pumped gas lasers is usually thought of in terms of the static voltage-current characteristic. Figure 26 depicts a typical case, and the negative resistance nature of the discharge becomes apparent through

$$R_i = \frac{dv}{di} < 0. \tag{19}$$

Drawing the loadline $v = V_b - iR$ in Fig. 26, we find

$$RI_o + v(I_o) = V_b. \tag{20}$$

From the perturbation check usually applied one could conclude that stability would merely require

$$R > \left| \frac{dv}{di} \right|_{i = I_o} = \left| R_i \right| \tag{21}$$

During the operation of various laser tubes, of the parameters characterized in Fig. 26, as well as tubes of shorter length, oscillatory instabilities in the frequency range from 150 to 500 kilocycles were observed, which defy the static stability criterion (20), and obviously represent a dynamic phenomenon in the discharge*. The observed oscillations can be explained on hand of the equivalent circuit of Fig. 27, which takes into account the inherent inductance, L, of the discharge, caused by ionization and deionization in the plasma**, as well as the parasitic capacity, C, of the electrode used for stabilization

---

* The oscillations occur for drive voltages V_b which are substantially lower than the ignition voltage of the tube, such that ordinary relaxation type oscillation definitely are ruled out.

** Ionization and deionization times are roughly equal in the geometries of interest, and their effect can be represented by an inductance, in the frequency range around 300 kilocycles.
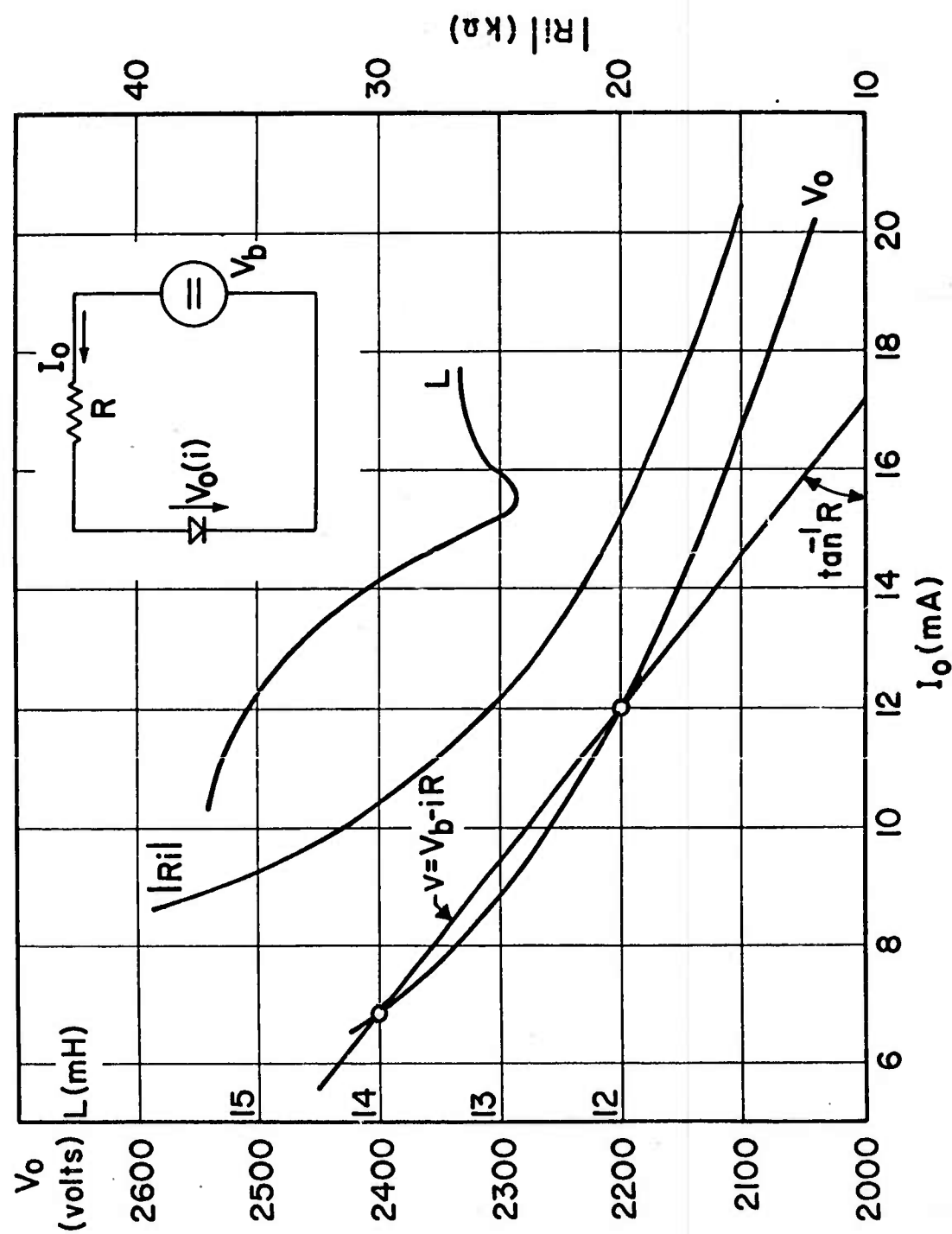
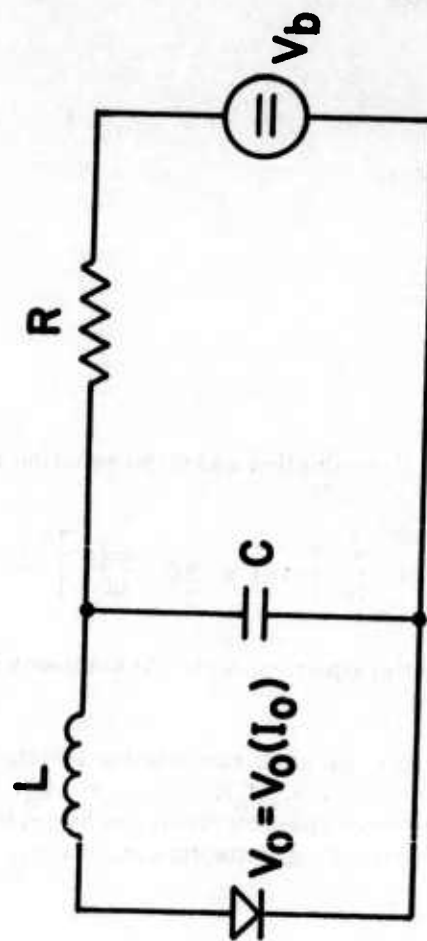Fig. 26 – Characteristic of a He-Ne discharge of 550 mm length and 2 mm diameter.

Fig. 27 – Equivalent circuit of the gas discharge and external drive and stabilizing network.

12331

and its associated circuitry. We can write

$$v(i) + L \frac{di_L}{dt} + iR = V_b \tag{22}$$

$$i = i_L + i_c \tag{23}$$

$$i_c = C \frac{d}{dt} (V_b - iR). \tag{24}$$

Combining (23) and (24) into

$$i_L = i + RC \frac{di}{dt} , \tag{25}$$

and by substituting i and di/dt, obtained by evaluation and differentiation of (22), into (25), we finally have

$$i_L + \frac{L}{R} \frac{di_L}{dt} + LC \frac{d^2 i_L}{dt^2} + \frac{1}{R} \left[v(i) + RC \frac{dv(i)}{dt} \right] = \frac{1}{R} V_b. \tag{26}$$

This represents a second order differential equation, which is nonlinear due to the terms $v(i)$ and $dv(i)/dt$.

To check stability of our equivalent circuit, we shall examine the effects of small perturbations of the steady state solution of (27), i.e., $I_o R - v(I_o) = V_b$. For small amplitude variations, the nonlinear discharge characteristic can be replaced by the first two terms of its Taylor expansion, corresponding to the tangent at $i = I_o$. Accordingly,

$$v = V_o + R_i (i - I_o), \quad R_i < 0. \tag{27}$$

Substitution of (27) into (26) renders a linear, second order differential equation, and its transient solution is composed of terms

$$i(t) = \left\{ \exp - \left[\frac{1}{2LC} \left(\frac{L}{R} + R_i C \right) t \right] \right\} x \begin{matrix} - \cos \omega_o t \\ \\ \sin \omega_o t \end{matrix} \tag{28}$$

- 54 -

with

$$\omega_o = \frac{1}{2LC} \sqrt{4LC \left(1 + \frac{R_i}{R}\right) - \left(\frac{L}{R} + R_i C\right)^2} \tag{29}$$

Stability corresponds to perturbations which decrease with time, and hence

$$\frac{L}{R} > \left|R_i\right| C. \tag{30}$$

At this point, since modulation of the discharge current will be of interest during the following discussion, let us also consider forced steady-state oscillations in the equivalent circuit of Fig. 27. Replacing V_b in (26) by $V_b + V_m \cos \omega t$, $V_m \ll V_b$, one readily finds the particular solution

$$I_m = \frac{V_m}{R} \frac{1}{\left[\left(1 - \frac{|R_i|}{R}\right) - \omega^2 LC\right] \cos \varphi - \omega\left(\frac{L}{R} - |R_i| C\right) \sin \varphi} \tag{31}$$

with

$$\tan \varphi = \frac{\omega\left(\frac{L}{R} - |R_i| C\right)}{\omega^2 LC - \left(1 - \frac{|R_i|}{R}\right)} . \tag{32}$$

This will produce a resonance at the frequency***

$$\bar{\omega}_o = \sqrt{\frac{\left(1 - \frac{|R_i|}{R}\right)}{LC}} = \omega_o, \; R \gg |R_i| . \tag{33}$$

*** This tacitly assumes that the expression under the square-root in (29) is positive. Otherwise, purely exponential rather than exponentially decaying oscillatory transients would result, and no resonance condition (35) can be specified for real ω_o.

For any given physical situation, the stabilizing resistor R will be the only quantity that one can more or less choose, except that obviously C should be minimized. This minimum value of the parasitic capacity, as well as L and R_i, are then characteristic constants for a specific design, while R has to satisfy the relation obtained from (21) and (30),

$$\frac{L}{\left|R_i\right| C} > R > \left|R_i\right|. \tag{34}$$

To compare various discharge geometries in view of their respective transient stability, we can choose a fixed margin of stabilization, expressed in a relation $R = \alpha \left|R_i\right|$, with $\alpha > 1$. Substituting into (30), this implies

$$\frac{L}{R_i^2} > \alpha\ C. \tag{35}$$

Since both L and $\left|R_i\right|$ are inversely proportional to the length of the plasma tube, and are proportional to the area of its cross-section, we conclude that transient stability of the discharge decreases with tube length and increases with area of the cross-section.

The results obtained are quite important in view of the possibility of direct amplitude modulation of the laser output, from the dc discharge current: Obviously, Eqs. (28) and (30) will determine the amount of ringing exhibited by the discharge. Figure 28 demonstrates the effect, for values of R which are quite low, from the viewpoint of static stabilization. A rough calculation of L and C, from the observed exponential decay and the ringing frequency, renders L = 14.4 mH and C = 13 pF.

Resonant tests performed on the discharge are summarized in Fig. 29, with an external capacity of 10 pF added across the discharge, to simulate an encapsulated tube. Values of external capacity ranging from 5 to 40 pF were also investigated and produced similar results. As was to be expected, resonance observed from the output of the differential amplifier was sharpest for the larger values of R, but also for decreasing discharge current I_o. Points determined experimentally for varying current I_o are marked in Fig. 29, with R being the parameter. For R = 50 k ohms and I_o = 13 mA, the circuit was found to be near free oscillation, and ω_o could be determined quite accurately. Substituted into (29) and (30), with an equality sign replacing the inequality sign, L and C were determined as L = 14.70 mH and C = 12.17 pF. The curve R = 40 k ohms was drawn in Fig. 29, and, using the smoothed values ω_o, L as a function of I_o was computed for C = 12.17, from (33). The resulting L(i) is shown in Fig. 26. With C and L(i) being specified, the rest of the curves were computed and drawn in Fig. 29. From the close agreement observed for the measured and computed performance, we may conclude that Fig. 27 represents an accurate representation of the discharge, at least within the frequency range covered in the experiments.

- 56 -
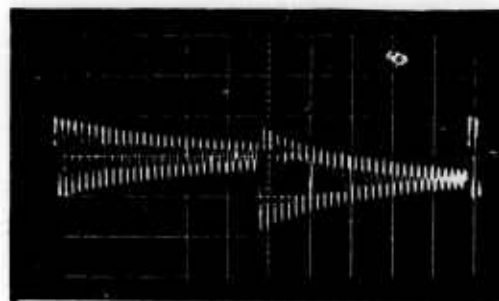
(a)
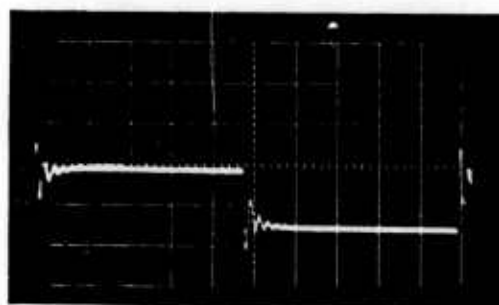
(b)
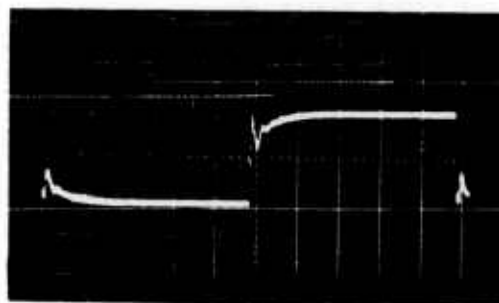
(c)

Fig. 28 - Oscillograph display for 5 kc squarewave modulation of the discharge current (a) $R = 5 \times 10^4$ (b) $R = 3.5 \times 10^4$, (c) $R = 2.5 \times 10^4$ Ohms. $I_C = 14$ mA sweep speed 20 μsec/cm.
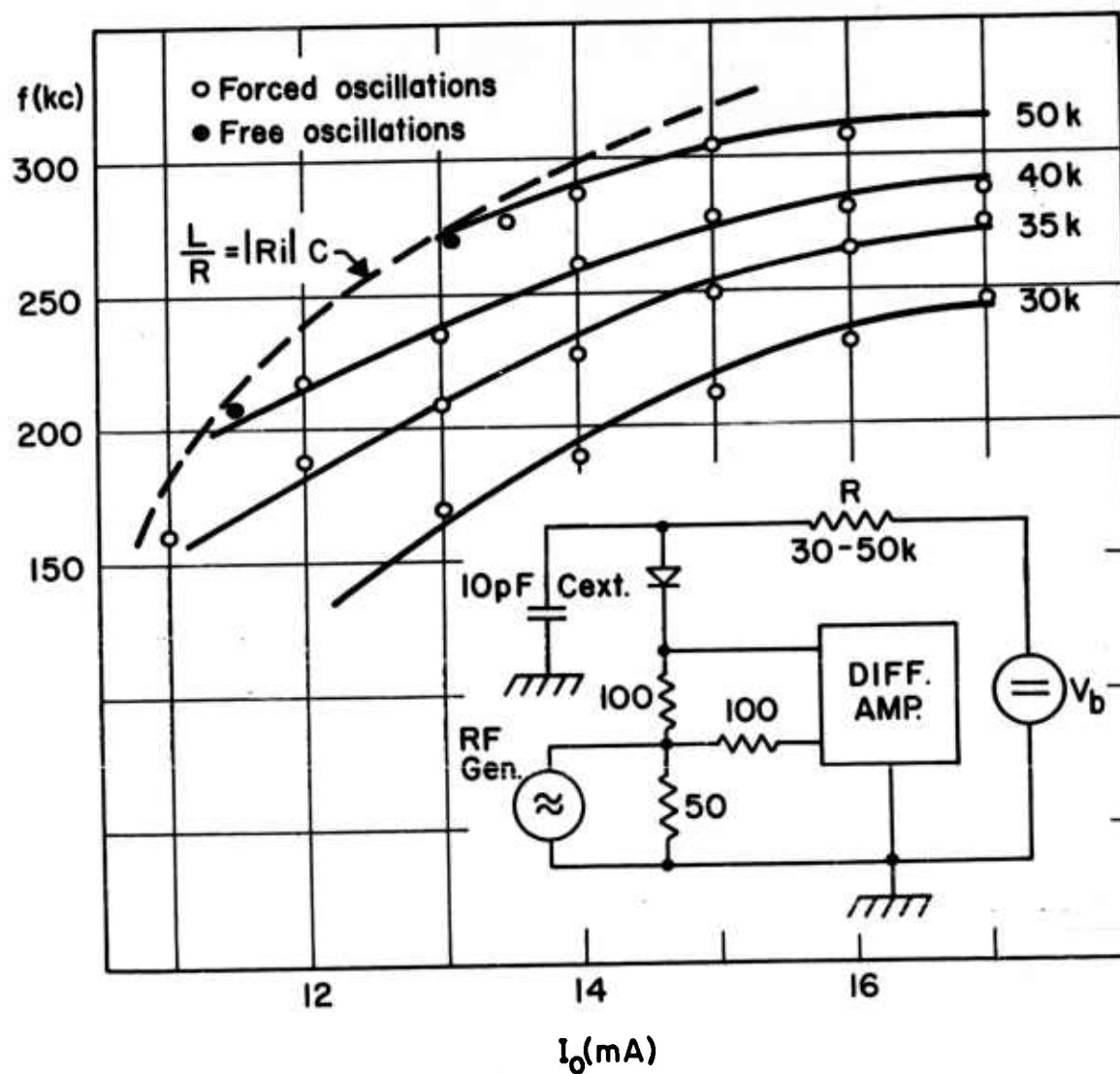
- 57 -

Fig. 29 - Resonance character of the discharge current, R parameter.

- 58 -

12330

The separatrix $L/R = |R_i| C$ drawn in Fig. 29 separates the region of transient stability from that of transient instability, in the I_o/f plane. Stable oscillations were observed on its left hand side, for the higher values of R, and agreement with the theory is excellent. Corresponding points are marked in Fig. 29. A typical waveform resulting for the discharge current is shown in Fig. 30, with the bottom line of the scale corresponding to zero current level. Stabilization of such stable oscillation relies on large signal effects, in the discharge, and proper limiting of its nearly sinusoidal waveform by the v(i) characteristic. It turns out that the condition of free oscillation is quite critical, and that its range is confined to the region immediately bordering on the separatrix. Normally, the oscillation grows to such large levels that its negative swing extinguishes the discharge, before stabilization by limiting can occur.

From the steady state solution for the discharge current and (27), or from (31) and (32) for $\omega = 0$, the static modulation characteristic of the discharge is readily obtained as

$$I_m = \frac{1}{R - |R_i|} V_m. \tag{36}$$

The modulating waveform $V_m \cos \omega t$ is thought to be superimposed on the battery voltage V_b, and in turn produces a modulation current $I_m \cos \omega t$, which is superimposed on I_o. If one thinks of V_m as a hum or drift voltage of the power supply, one concludes that $R \gg |R_i|$ would render minimum fluctuations of the discharge.

According to the restrictions imposed on R by (30) and (34), we clearly have to make a compromise between transient stability and ringing of the discharge on one hand, and adequate filtering and regulation of the power supply on the other.

To take into account the effects of L and C, the modulation transconductance, $G_m = I_m/V_m$ computed from (31) and plotted as a function of frequency is shown in Fig. 31. The progressive resonance character with increasing R becomes apparent, and for $R = 50$ k ohms the effect is quite pronounced.

To estimate the resulting optical modulation produced by amplitude variation of the dc-discharge current, we would not only have to establish the optical power versus discharge current characteristic for the laser, but also its optical oscillator transient nature. It has been observed that, while the optical output seems to follow increases in discharge current in times of the order of tenths of microseconds, the longer lifetime of the helium metastables casues a certain prolongation**** of the light output after reduction of the discharge current, from values close to maximum power output. It was not the purpose of the foregoing consideration to investigate these effects, and we have merely attempted to present a clarification of the transient and steady state contributions arising from the discharge.

**** S. E. Sobottka, private communication.

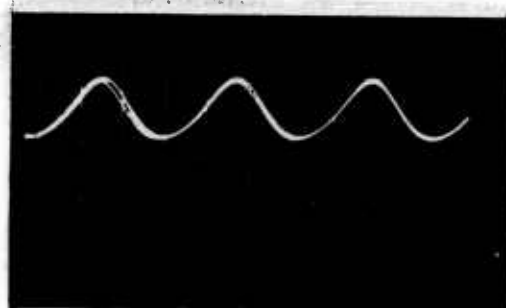Fig. 30 - Display of the steady state oscillation observed.
$R = 2 \times 10^4$, $C_{ext} = 40$ pF, $I_O = 20$ mA; sweep 2 μsec/cm,
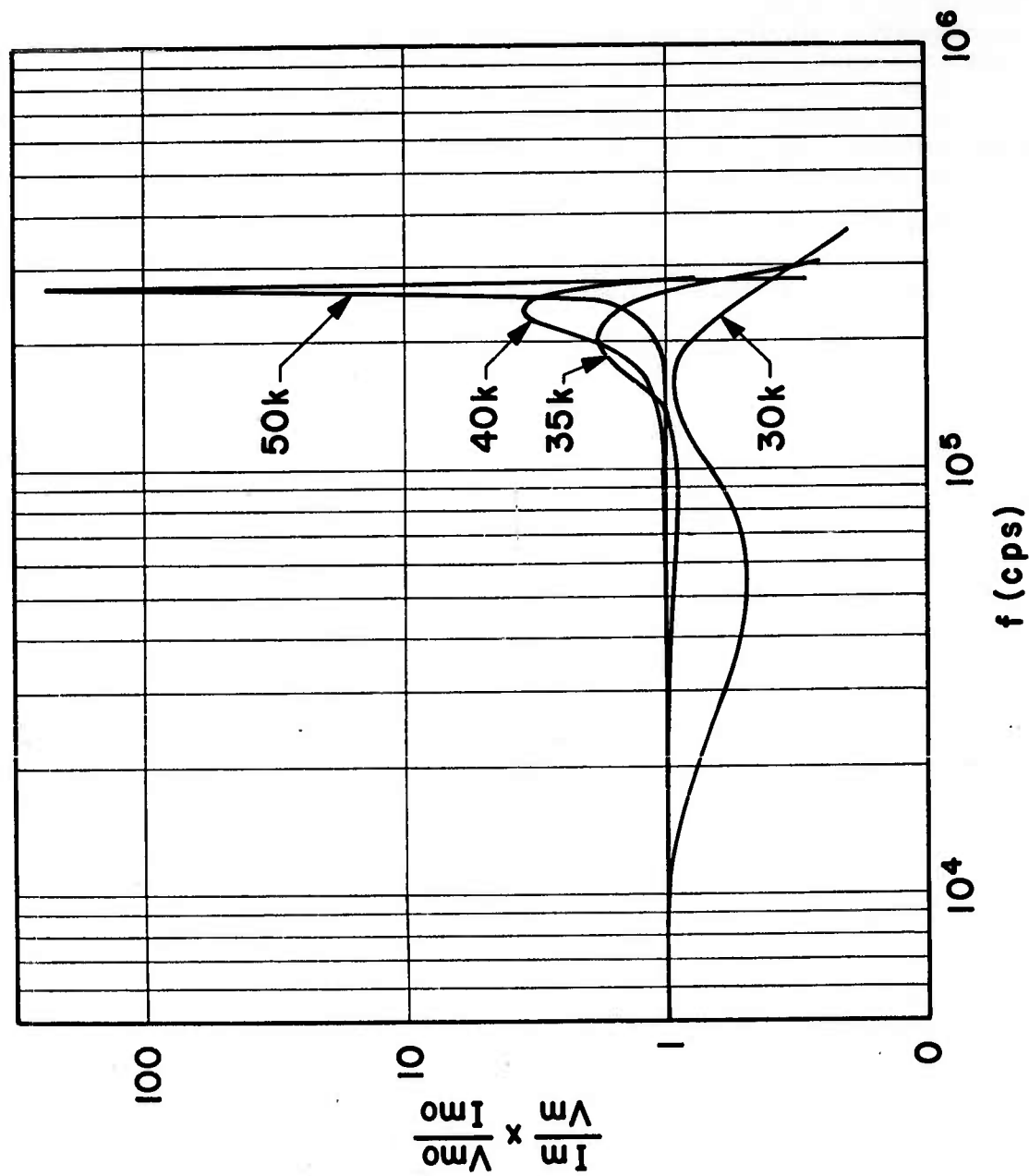4.75 mA/cm.

Fig. 31 - Modulation characteristic of the discharge of Fig. 26.

- 61 -

12328

APPENDIX III

GEOMETRIC ARRANGEMENT TO REDUCE THE EFFECTIVE
ELECTRON-DENSITY WITHIN THE MODE VOLUME

The considerations that prompted the design of the gridded tube, i.e., that saturation observed in an He-Ne laser was due to overpopulation of the lower laser levels caused by electron collisions, while the upper laser level population was hoped to be proportional to the discharge current and the electron density, led to the design and construction of the experimental tube shown in Fig. 32. Also, Fig. 33 shows the axial distribution of the anticipated electron and atomic densities, on a qualitative basis. It is quite plausible, that in the gaps the electrons follow the lines of electric field and diffuse quite rapidly towards the walls, causing a pronounced dip in the electron density. This is readily verified from an inspection of the discharge in the periodic structure. Motion of the electrically neutral helium metastables and excited neon atoms is described by the usual diffusion laws, and a much smaller dip in relative density will be observed, if the extnesion of the gap in the z- direction does not exceed the diameter of the plasma tube. In the gaps, on the other hand, the electron density is only one tenth or less of that in the unrestricted portions of the tube. The beneficial effect of the absence of electron, in a portion of the mode volume, if existant, should then become apparent in a gain measurement.

Although the densities of excited atoms decrease in the gaps, the absence of electrons would have rendered a relative decrease in population of the lower laser level, and should have produced a higher population inversion that encountered the high current density sections of the tube. If the provision of a sufficient number of gaps would thus yield a net increase in population inversion for a given length of tube, then overall gain would also be increased over a smooth-wall tube, and higher output power should result.

The construction of the experimental tube shown in Fig. 32 permitted an evaluation of the increased gain through reduced electron density concept, by direct comparison of a smooth wall with a corrugated wall section of idential total length, as shown.

Tube and cavity were laid out entirely symmetrical, and with the corresponding half of the tube excited, differences in small signal gain were observed by comparing the lasing output obtained near oscillation threshold, both at the 6328Å as well as the 1.15 μ wavelength. It was observed that the corrugated section produced slightly less but practically equal small signal gain and power output over the large ranges of pressures, He-Ne mixtures and dc currents investigated. This still is a significant result, since the right half in Fig. 32, although of identical overall length, has one third of its wall missing.
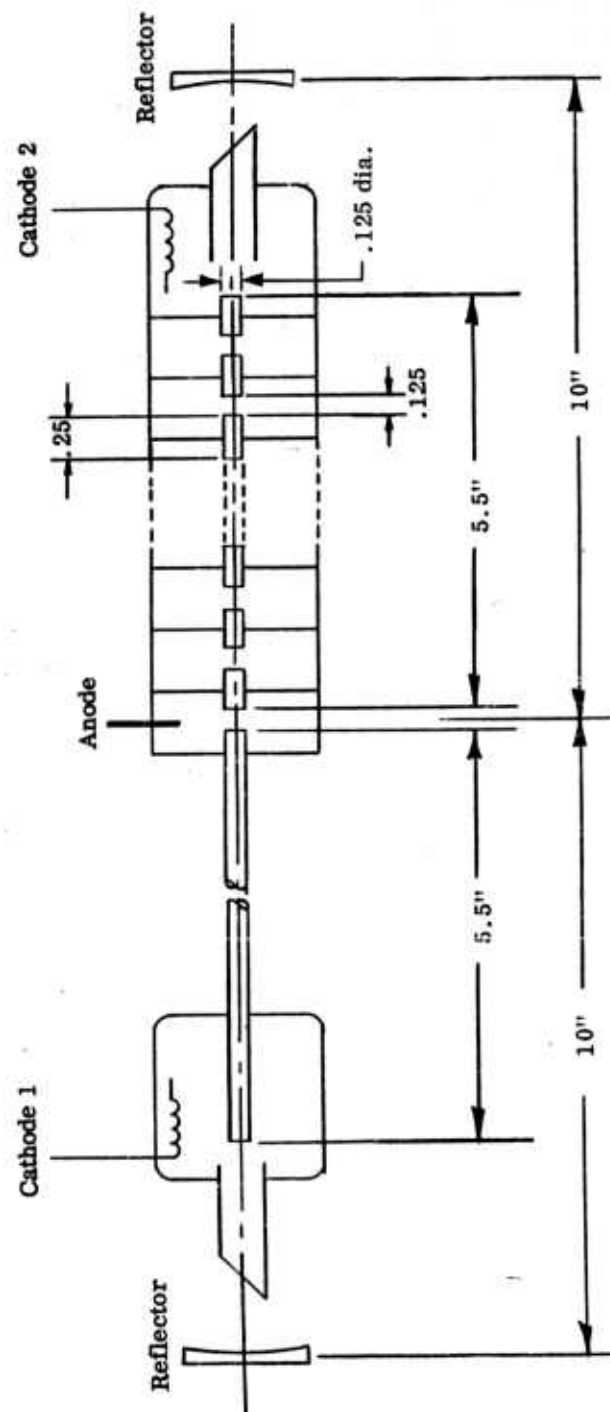
- 62 -

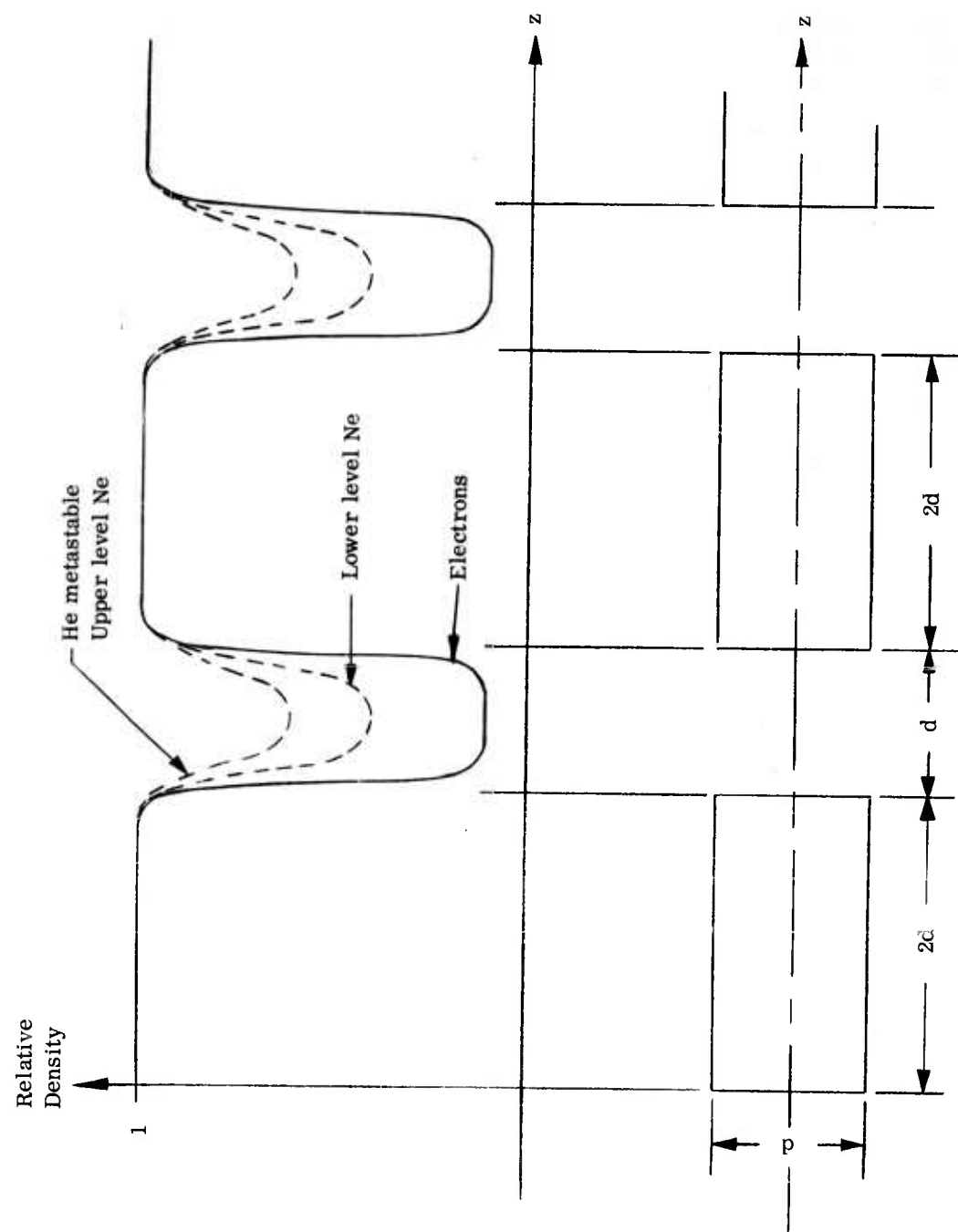Fig. 32 – Experimental tube featuring smooth wall and periodic gap sections of equal total length.

Fig. 33 - Axial distribution of the electron and He-Ne densities in the corrugated wall tube.

- 64 -

Although it appears plausible that the absence of electrons in part of the mode-volume produces a beneficial effect, this effect does not sufficiently counteract the reduction in gain caused by the reduced densities of Hc and Ne atoms to produce an overall increase. Since the atomic density reductions in the gaps are estimated to correspond to a factor not smaller than one half, the beneficial effect is in turn estimated to correspond to a factor of two or less. This agrees well with the observations of power output in the afterglow reported in the literature.

DISTRIBUTION LIST

Contract No. AF 33(657)-8986

Activities at Wright-Patterson AFB	No. of Copies
SEPRR (Library)	1
SEPR (Tech. Reports Division)	1
AVTP	5

Other Department of Defense Activities

Air Force

Commander
Air Force Cambridge Research Laboratories
Attn: CRRS (Mr. R. W. Wagner)
L. G. Hanscom Field
Bedford, Massachusetts   1

Army

Commanding Officer
U. S. Army Electronics Research Laboratories
Electron Devi es Division
Attn: Mr. Harold J. Hersh
Fort Monmouth, New Jersey   1

Commanding Officer
Diamond Ordnance Fuze Laboratories
Attn: Mr. J. H. VanTrump (1 copy)
        Dr. Robert T. Your ; (1 copy)
Microwave Tube Brar ch
Washington 25, D.C.   2

Distribution List (continued)

Other U. S. Government Agencies	No. of Copies

Advisory Group on Electron Devices
Attn: Mr. H. N. Serig
346 Broadway, 8th Floor
New York 13, New York   4

DDC
Cameron Station
Alexandria, Virginia   22314   20

Non-Government Individuals and Organizations

Autonetics, A Division of NAA, Inc.
9150 East Imperial Highway
Downey, California   1

General Motors Corporation
Defense Systems Division
Santa Barbara, California   1

General Electric Company
118 West First Street
Dayton 2, Ohio   1

General Telephone and Electronic Labs., Inc.
Bayside, New York   1

Hughes Research Laboratories
Malibu, California   1

International Business Machines Research Center
Yorktown Heights, New York   1

Maser Optics, Inc.
89 Brighton Avenue
Boston 34, Massachusetts   1

Distribution List (continued)

Minneapolis-Honeywell Company
1441 Milburn Avenue
Dayton 4, Ohio   1

Martin-Orlando
Attn: A. Vuylsteke
Orlando, Florida   1

Massachusetts Institute of Technology
Boston, Massachusetts   1

Ohio State University Research Foundation
1314 Kinnear Road
Columbus 12, Ohio   1

Radio Corporation of America
Princeton Lab
Princeton, New Jersey   1

Raytheon Company
Research Division
Waltham, Massachusetts   1

Sperry Gyroscope Company
Attn: Dr. G. White
Great Neck, New York   1

TRG, Inc.
Technical Research Group
2 Aerial Way
Syosset, New York   1

Electro-Optical Systems, Inc.
125 North Vinedo Avenue
Pasadena, California   1

Distribution List (continued)

Harrison M. Randall Laboratory of Physics University of Michigan Ann Arbor, Michigan	1
S-F-D Laboratories, Inc. 800 Rahway Avenue Union, New Jersey	1
Stanford Research Institute Menlo Park, California	1
Varian Associates 611 Hansen Way Palo Alto 63, California	1
Quantatron, Inc. 2520 Colorado Avenue Santa Monico, California	1
Massachusetts Institute of Technology Lincoln Laboratory Lexington 73, Massachusetts Attn: Mary A. Granese, Documents Librarian	1
Laboratory for Electronics, Inc. 1079 Commonwealth Avenue Boston 15, Massachusetts Attn: Mrs. A. Cakste, Librarian	1